Title	An experimental and kinetic modeling study of cyclopentane and dimethyl ether blends
Author(s)	Lokachari, Nitin; Wagnon, Scott W.; Kukkadapu, Goutham; Pitz, William J.; Curran, Henry J.
Publication Date	2020-11-13
Publication Information	Lokachari, Nitin, Wagnon, Scott W., Kukkadapu, Goutham, Pitz, William J., & Curran, Henry J. (2021). An experimental and kinetic modeling study of cyclopentane and dimethyl ether blends. Combustion and Flame, 225, 255-271. doi:https://doi.org/10.1016/j.combustflame.2020.10.017
Publisher	Elsevier
Link to publisher's version	https://doi.org/10.1016/j.combustflame.2020.10.017
Item record	http://hdl.handle.net/10379/16483
DOI	http://dx.doi.org/10.1016/j.combustflame.2020.10.017

An experimental and kinetic modeling study of cyclopentane and dimethyl ether blends

Nitin Lokachari[1], Scott W. Wagnon[2, *], Goutham Kukkadapu[2], William J. Pitz[2], Henry J. Curran[1]

[1] Combustion Chemistry Centre, School of Chemistry, Ryan Institute, MaREI, National University of Ireland, Galway, Ireland

[2] Materials Science Division, Lawrence Livermore National Laboratory, Livermore, CA 94551, USA

* **Corresponding author**

Scott W. Wagnon
Material Science Division
Lawrence Livermore National Laboratory
7000 East Avenue
Livermore, CA 94550
USA
Email: wagnon1@llnl.gov
Phone: +1-925-422-2819

Type of article: Full length

For printed editions, the authors request that color figures are converted to black and white.

Abstract

Cyclopentane is a suitable naphthene, or cycloalkane, in a palette for multi-component gasoline surrogate fuels due to its presence in market fuels and its relevance to alkyl substituted cyclopentanes also present. However, the previous oxidation studies of cyclopentane have primarily focused on neat mixtures. Blending cyclopentane with dimethyl ether in this work therefore serves to inform our understanding of, and improve predictive models for, multi-component mixtures. In this work, the auto-ignition of cyclopentane/dimethyl ether blends was studied in a high-pressure shock tube and a rapid compression machine. A wide range of temperatures (650 – 1350 K) and elevated pressures of 20 and 40 bar were studied at equivalence ratios of 0.5, 1.0 and 2.0 in air for two blending ratios (30/70 and 70/30 mole % cyclopentane/dimethyl ether mixtures). A detailed kinetic model for cyclopentane was revised to capture the measured ignition delay times and apparent heat release rates in this study. Literature ignition delay time, jet-stirred reactor, and laminar burning velocity measurements of neat cyclopentane were used as additional validation. Improvements to the kinetic model were based on recent literature studies related to sub-models including cyclopentene and cyclopentadiene which allowed the removal of previous local rate-constant optimizations. Low temperature reactivity of cyclopentane was found to be controlled by the branching ratio between concerted elimination of $H\dot{O}_2$ and the strained formation of $\dot{Q}OOH$ radicals in agreement with previous studies. In this study, the low branching ratio of $\dot{Q}OOH$ formation increases the influence of a competing consumption pathway for cyclopentyl-peroxy, $CPT\dot{O}_2J$. The sensitivity of the simulated ignition delay times to the formation of cyclopentyl hydroperoxide ($CPTO_2H$), from $CPT\dot{O}_2J$ and $H\dot{O}_2$, is discussed. The current model is used to analyze the influence of dimethyl ether on the reactivity

of cyclopentane in the context of previous literature studies of dimethyl ether binary blends with ethanol and toluene.

Keywords: cyclopentane, gasoline surrogates, chemical kinetics, shock-tube, rapid compression machine

1. Introduction

Cyclopentane (CPT), the smallest typical cycloalkane compound present in commercial fuels, can be used to represent the naphthene class in multi-component surrogate fuels. The concentration of cycloalkanes in commercial ground and aviation fuels varies from 5 – 40% by volume [1]. However, as the utilization of non-conventional resources such as oil sands and biomass increases, the concentration of cycloalkanes may be significantly higher in comparison to those derived from crude oil [2, 3]. Such changes in fuel composition may also impact other regulated emissions such as soot. It is likely that cycloalkanes generate more intermediates, including aromatics and polycyclic aromatics that lead to soot formation relative to acyclic alkanes [4, 5]. Hence, cyclopentane is of interest to the combustion community.

Recently, Al Rashidi et al. [6] measured intermediate species during cyclopentane oxidation in a jet-stirred reactor (JSR), reported fundamental ignition delay times (IDTs), and developed a kinetic model for neat CPT [7]. Randazzo et al. [8] and Khandavilli et al. [9] have studied the pyrolysis of cyclopentane at various conditions in a shock-tube (ST) and in a continuous flow tubular reactor. Various literature studies that have provided valuable insights into the combustion behavior of neat cyclopentane and are listed in Table 1.

Table 1. Experimental measurements of neat cyclopentane data available in the literature.

Experiment	Conditions	Composition	Reference
Flame speed (counterflow twin flame)	1 atm $T_u = 298 - 453$ K	CPT in air $\varphi = 0.7 - 1.7$	Davis et al. [10]
Flame speed (spherically propagating flame)	1, 2, 5 atm $T_u = 403$ K	CPT in air $\varphi = 0.7 - 1.6$	Zhao et al. [11]
Ignition delay time (ST)	1, 10 atm $T_5 = 1150 - 1850$ K	1% CPT/O_2 in Ar $\varphi = 0.57, 1.0, 2.0$	Tian et al. [12]
Ignition delay time (ST)	7, 9 atm $T_5 = 1230 - 1840$ K	0.5–1.0% CPT/O_2 in Ar $\varphi = 0.5 - 2.0$	Sirjean et al. [13]
Ignition delay time (ST)	11 – 61 atm $T_5 = 1230 - 1840$ K	CPT in air $\varphi = 0.5 - 2.0$	Daley et al. [14]
Ignition delay time (RCM)	20, 50 bar $T_C = 700 - 980$ K	CPT in 12 – 21% O_2 $\varphi = 1.0$	Fridlyand et al. [15]
Ignition delay time (ST & RCM)	20, 40 bar $T_C = 675 - 1300$ K	CPT in air $\varphi = 0.5 - 2.0$	Al Rashidi et al. [7]
Species measurements (JSR)	1 atm $T = 900 - 1250$ K	CPT = 1000 ppm $\varphi = 0.5 - 2.0$	Dayma et al. [16]
Species measurements (JSR)	10 atm $T = 750 - 1250$ K	CPT = 1000 ppm $\varphi = 0.5 - 3.0$	Al Rashidi et al. [6]
Pyrolysis (Flow reactor)	$\tau = 0.5$ s $T = 973 - 1073$ K	1.7 bar	Khandavilli et al. [9]

It is evident from the available literature that the blending behavior of cyclopentane is not well established. It is important to understand the auto-ignition behavior of cyclopentane in fuel mixtures given its relevance to market fuel components and as a palette component for multi-component surrogate fuels [17, 18]. Cyclopentane has also seen interest as a blending component in gasolines as an octane enhancer. As a neat component, CPT has a research octane number (RON) of 103 and an octane sensitivity (OS = RON – MON) of 18 which are partially explained by the longer ignition delay times reported in the literature [7, 15]. In this study, we attempt to

understand (i) the low temperature auto-ignition of neat CPT and (ii) the auto-ignition behavior of CPT in binary mixtures containing dimethyl ether (DME).

DME is a suitable component to blend with unreactive fuels such as CPT because it has a reactivity that is representative of compounds in gasoline like *n*-heptane. Also, DME is a small volatile component whose combustion chemistry is relatively well understood while exhibiting negative temperature coefficient (NTC) behavior characteristic of reactive compounds. The interaction of CPT with the ȮH radical pool generated from the low temperature chemistry of DME is also relevant to understanding the role of CPT in gasoline mixtures which typically exhibit NTC behavior.

Previously, Zhang et al. took a similar approach to probe the low temperature reactivity of ethanol [19] and toluene [20] in blends with DME. These studies provided additional insights into the reactivity of these components and their mixtures while also improving the predictability of their respective kinetic models. The IDT experiments in this work were performed in high-pressure shock tube (HPST) and rapid compression machine (RCM) facilities at NUI Galway (NUIG), over a wide range of conditions, covering three equivalence ratios $\varphi = 0.5$, 1.0 and 2.0 in synthetic air (i.e. the mol. ratio of $N_2:O_2 = 3.76$), in the temperature range 650 – 1350 K at pressures of 20 and 40 bar for two binary compositions of 30/70 and 70/30 CPT/DME by mole percentage. The following manuscript is organized by first providing a brief overview of the experimental methodologies in Section 2, followed by a detailed description of our kinetic modeling updates to the CPT chemistry in Section 3. A discussion of the important findings from this study follows in Section 4 and a summary along with recommendations for future work are presented in Section 5.

2. Experimental Methodologies

Fuel-air mixture preparation and experimental uncertainty

The binary mixtures prepared for this study had fixed concentrations of O_2 and N_2 as found in air. Cyclopentane (99%) and DME (99.5%) were obtained from Sigma-Aldrich, while O_2 (99.99%), N_2 (99.99%) and helium (He) (99.97%) were supplied by BOC Ireland. The experimental conditions are listed in Table 2. For the mixture preparation, both fuels, O_2 and N_2 were added in the order of increasing partial pressures. The temperature of the mixing tank and the connecting lines was maintained at 50 $^\circ$C to prevent fuel condensation. The partial pressures of the fuels were maintained at a pressure at least a factor of three lower than the corresponding saturation vapor pressure at a given temperature. Fuel mixtures were diffusively mixed for at least 6 hours to achieve homogeneity. Both the shock-tube and rapid compression machine facilities have some uncertainties in their experimental measurements. The major uncertainties in the HPST experiments are attributed to shock velocity measurements, the diaphragm bursting mechanism, and boundary layer formation behind the incident shock wave, which is a facility effect. Petersen et al. [21] quantified the uncertainty in the temperature behind the reflected shock wave (T_5) using an estimated uncertainty in the measured incident shock velocity. A similar approach, using a 1-D equation for reflected shock temperature, which is a function of the initial temperature (T_1), the gas specific heat ratio (γ) and Mach number (M), was adopted for uncertainty quantification of the reflected shock temperature in the HPST experiments performed at NUIG [22]. It was reported that uncertainties change with operational conditions such as the compressed temperature and pressure conditions. The uncertainty in the time interval recorded by the pressure sensors was estimated to be ± 1 μs and the uncertainty in the position of the pressure sensor was estimated to be ± 0.1 mm. These uncertainties affect the uncertainty in the

measurement of the shock velocity. The average uncertainties in T_5 and IDT measurement using the NUIG HPST are $\pm$ 5 K and ~20% in the temperature range 1000 – 1500 K. Similarly, to estimate the uncertainty in the calculated compressed temperature in RCMs Weber et al. [23] developed a Monte Carlo method. The python scripts developed by Weber et al. were used and the uncertainties in T_C and IDT measurements were reported to be in the range of $\pm$ 5 – 10 K and $\pm$ 20 – 25%, respectively, in the temperature range 650 – 950 K. More details regarding the uncertainty measurements in the NUIG facilities have already been published [22].

High Pressure Shock Tube (HPST) - NUIG

High temperature (900 – 1350 K) IDTs of the CPT/DME blends were measured behind reflected shock waves, where the auto-ignition time scales range from 0.03 – 6.5 ms. A 30 cm double-diaphragm section separates the 9 m long steel tube of uniform cross-section of 63.5 mm inner diameter into a 3 m driver section and a 5.7 m driven section.

Table 2. Experimental conditions of the binary mixture compositions (in mole fraction) investigated in this study.

φ	CPT	DME	O_2	N_2	p_C (bar)	T_C (K)	Facility
0.5	0.012	0.005	0.206	0.777			
0.5	0.007	0.016	0.205	0.771			
1.0	0.023	0.010	0.203	0.764			
1.0	0.014	0.032	0.200	0.754	20 and 40	650 – 1350	RCM/HPST
2.0	0.045	0.019	0.197	0.739			
2.0	0.026	0.062	0.192	0.720			

The driven section is filled with the CPT/DME binary gas mixture and the driver section with a lighter non-reactive gas, helium. However, for the tests involving longer ignition times (2

– 6 ms), He is partly replaced with N_2 to optimize the interaction of the reflected shock with the contact surface at the endwall.

When the double diaphragm bursts, a shock wave, formed by expansion of the driver gas, propagates at supersonic speeds through the driven section. This propagating front rapidly compresses and heats the test gas to the desired thermodynamic conditions at the endwall before auto-ignition. By varying the Mach number of the shock wave, the final compressed pressure and temperature conditions of the test gas are varied. Six piezoelectric pressure transducers (PCB 113B24) are mounted on the sidewall of the driven section to record the time of arrival of the incident shock, which are required to measure the shock velocity at the endwall. The compressed pressure and temperature are calculated using the "reflected shock" routine in Gaseq [24]. A dynamic pressure transducer (Kistler 603B) mounted at the endwall records the pressure history of the test gas from which the IDTs are measured. The pressure signals are recorded using Tie-pie handyscope HS4-50 digital oscilloscopes at 12-bit resolution and the acceptable uncertainty for the measured pressures behind the reflected shocks are limited to $\pm 5\%$.

Rapid Compression Machine (RCM) - NUIG

The low temperature (650 – 900 K) IDTs of CPT/DME blends were measured in an RCM at compressed pressures of 20 and 40 bar. This RCM facility has a 38 mm bore and 168 mm stroke and uses opposed twin pistons to quickly compress (12 – 14 ms) the test gas mixture to the desired thermodynamic states. The creviced pistons, that largely limit the turbulence/roll-up vortices generated in the test gas, are pneumatically driven and mechanically locked at the end of compression. Having a homogeneous temperature of the compressed fuel/air mixture inside the reaction chamber (RC) is critical, as the rate of reaction depends exponentially on temperature,

and in-homogeneities can complicate the interpretation of experimental results. A recent computational study [25] characterized the flow fields inside the RC of the NUIG RCM, and the results indicated that the piston crevice suppresses the roll up vortex and produces a largely uniform temperature field in RC at the end of compression, to post-compression times of approximately 150 ms. After compression, the pressure drops due to heat transfer from the gas mixture to the reaction chamber walls. Time-resolved pressure measurements are recorded using a piezoelectric pressure sensor (Kistler 6045A) mounted on the sidewall of the reaction chamber. The initial temperature and pressure, mixture composition and compressed gas pressure of each experiment are all used to determine the compressed gas temperature using the "adiabatic compression/expansion" routine in Gaseq [24]. Pyrolytic experiments are conducted by replacing O_2 in the test mixture with N_2 to create effective volume histories as input for simulations that capture compression and heat transfer effects.
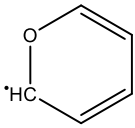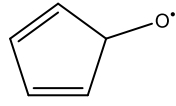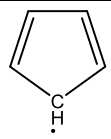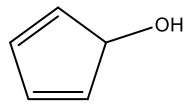
3. Chemical kinetic modeling
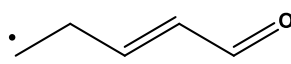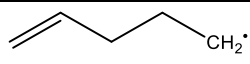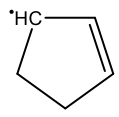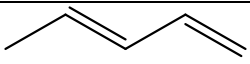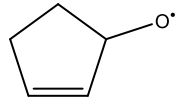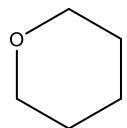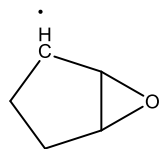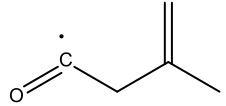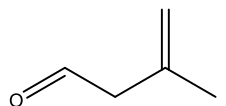
3.1 Preliminary model formulation
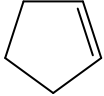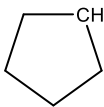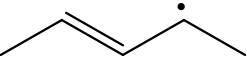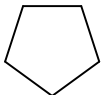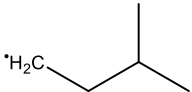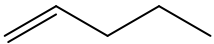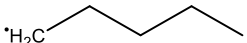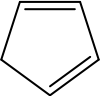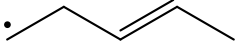
The current chemical kinetic model for cyclopentane was developed from the basis of a small hydrocarbon ($C_0 - C_4$) kinetic model from NUIG [26] and previous kinetic model of cyclopentane by Al Rashidi et al. [27]. Aromatic chemistry stemming from cyclopentadiene and cyclopentadienyl pathways was required and included from the study by Kukkadapu et al. [28]. As part of this work a critical re-evaluation of the cyclopentane, cyclopentene, cyclopentadiene and dimethyl ether sub-models was undertaken and will be discussed in the following sections. Additional comments and citations can be found next to each relevant reaction in the kinetics mechanism file in the supplemental material for those not explicitly discussed in the main text.

If available and accurate, thermochemistry of a species was taken from the references above. If new or updated thermodynamic properties were needed for a species, Benson's group additivity methods as implemented in THERM [29] were applied to estimate properties (i.e. enthalpy, entropy, heat capacity). Table 3 presents a comparison of thermodynamic properties for cyclopentane and C_5 intermediates modified in this work relative to the values reported in the kinetic model of Al Rashidi et al. [27]. Group values used in this work come from the review and optimizations by Burke et al. [30] and Li et al. [31]. Additional groups, such as ring corrections, from Ritter and Bozzelli [29] were also used. Transport properties for the small hydrocarbon species were included from the NUIG model [26]. New transport properties for larger species unavailable from previous work were estimated using the approach described in Wagnon et al. [32] with correlations from Dooley et al. [33] and Bosque and Sales [34]. Simulations of IDTs utilized the Lawrence Livermore National Laboratory (LLNL) developed software ZeroRK [35], including non-reactive volume histories for the RCM experiments and a constant volume approximation for ST experiments. Additional literature experiments (e.g. jet-stirred reactor, flame speeds) were simulated using the appropriate CHEMKIN-Pro modules.

Table 3. Enthalpy (H), entropy (S), and heat capacity (Cp) of cyclopentane and select C5 intermediates from a) the current work and b) Al Rashidi et al. [27]. Note, only species with differences larger than 0.4 kcal/mol or cal/mol/K are presented.

2D depiction	model name	H(298K)a	S(298K)a	Cp(300K)a	H(298K)b	S(298K)b	Cp(300K)b
		[kcal/mol]	[cal/mol/K]	[cal/mol/K]	[kcal/mol]	[cal/mol/K]	[cal/mol/K]
	cyC₅ODEJ	21.95	66.44	21.4	8.8	66.45	21.44

	Species	Value 1	Value 2	Value 3	Value 4	Value 5	Value 6
(structure: cyclopentadienyl with O radical)	$C_5H_5\dot{O}$	50.36	73.71	22.38	43.35	71.38	21.13
(structure: cyclopentadienyl radical with CH at bottom)	$\dot{C}_5H_5$	62.53	63.48	20.7	57.18	63.59	17.97
(structure: cyclopentadiene with OH)	C_5H_5OH	−1.81	75.41	22.22	−9.02	75.34	22.1
(structure: open chain with radical and aldehyde O)	$\dot{C}_4H_6CHO2-5$	20.55	90.6	26.38	16.16	88.52	26.92
(structure: pentenyl chain with CH₂ radical)	$\dot{C}_5H_91-5$	43.7	86.08	25.54	44.06	80.9	26.23
(structure: cyclopentene with HC radical)	$cy\dot{C}_5H_71-3$	39.58	69.57	19.6	40.71	67.98	16.2
(structure: pentadiene chain)	C_5H_81-3	18.74	76.85	24.36	16.4	74.99	24.8
(structure: cyclopentene with O radical)	$cyC_51EN3\dot{O}J$	20.24	77.04	24.19	22.01	77.65	23.09
(structure: tetrahydropyran)	$C_5H_{10}O1-5$	−54.09	71.87	23.08	−54.71	71.86	25.82
(structure: bicyclic epoxide with CH radical)	CPTYO123J	25.82	68.32	19.34	26	67.72	17
(structure: methyl branched with C radical and O)	$iC_4H_7\dot{C}O$	9.16	88.97	25.16	10.4	89.37	26.32
(structure: methyl branched aldehyde)	iC_4H_7CHO	−27.74	87.85	26	−26.5	88.25	27.15

cyC$_5$H$_8$	7.51	69.47	20.14	9.65	69.42	19.71
cyĊ$_5$H$_9$	26.91	71.49	20.3	26.6	71.97	22.03
Ċ$_5$H$_9$2-4	25.61	79.37	24.65	25.74	77.64	24.31
CPT	−19.09	69.77	20.32	−18.89	70.01	19.58
dĊ$_5$H$_{11}$	12.73	85.82	28.12	12.3	85.46	27.87
C$_5$H$_{10}$-1	−5.35	82.77	26.67	−5.02	82.67	26.09
Ċ$_5$H$_{11}$-1	14.03	88.49	28.13	14.46	88.16	27.92
C$_5$H$_6$	32.1	65.53	18.21	31.26	65.51	18.32
Ċ$_5$H$_9$2-5	41.5	85.46	24.83	41.42	85.06	25.31

3.2 Cyclopentane sub-model

A summary of the reactions and associated rate constants from the current kinetic sub-model for cyclopentane is presented in Table 4. Unimolecular fuel decomposition via the carbon-carbon bonds in cyclopentane has long been thought to proceed primarily via the formation of a di-radical and prompt H-atom transfer forming 1-pentene [8, 36, 37]. An alternative unimolecular decomposition involving the carbon-carbon bonds leads to the formation of ethylene and

LLNL-JRNL-811439-DRAFT

cyclopropane [8, 36, 37]. In the current study, the CBS-QB3 rate constants calculated by Sirjean et al. [36] were adopted for both pathways which are generally in reasonable agreement with other literature studies as noted by Randazzo et al. [8]. Further resolving and refinement of these unimolecular pathways and reaction rates likely requires calculations utilizing multi-reference methods, as applied in the ring-opening of cyclohexane [38]. Loss of an H-atom from cyclopentane to form a cyclopentyl radical is written in the reverse direction using an estimated rate constant of 1×10^{14} cm^3 mol^{-1} s^{-1}, which is common for such termination reactions. Cyclopentane models would benefit from high accuracy, pressure dependent evaluations of these unimolecular reactions that extend to conditions relevant to modern internal combustion engines $(500 - 2500$ K, $1 - 100$ bar$)$.

H-atom abstraction reactions from cyclopentane by small radicals such as $\dot{H}$, $\ddot{O}$, and $\dot{O}H$ were taken from previous experimental and theoretical studies [39-41]. Rate coefficients for the H-atom abstractors O_2, $H\dot{O}_2$, and $\dot{C}H_3$ have not been studied experimentally or computationally for cyclopentane to the authors' knowledge and are excellent candidates for future work. Currently, H-atom abstraction by molecular oxygen was estimated using a rate constant rule of the $A = n \cdot 9 \times 10^{13}$ cm^3 mol^{-1} s^{-1} and $E = \Delta H + 2 \cdot R \cdot (1000\ K)$ cal mol^{-1}. For the rate constant rule, A is the pre-exponential factor, E is the activation energy, n is the number of equivalent hydrogen atoms available, ΔH is the enthalpy of the reaction, and R is the molar gas constant. This proposed rule builds on observations beginning as early as the 1970s, where R.W. Walker and other researchers [42] recognized that a constant A-factor on a per hydrogen basis and an activation energy approximately equal to the enthalpy of reaction were reasonable approximations to describe $RH + O_2 = \dot{R} + H\dot{O}_2$ in Arrhenius form. Like Walker and colleagues, the proposed rate constant rule in this work establishes the common A-factor based on

formaldehyde, $CH_2O + O_2 = H\dot{C}O + H\dot{O}_2$ [43], and some comparisons of the rule to literature calculations of other species are provided in the Supplementary Material. Abstraction of H-atoms by $H\dot{O}_2$ radicals was assumed to be analogous to abstraction from secondary alkyl sites as calculated by Aguilera-Iparraguirre et al. [44] multiplied by the number of equivalent hydrogen atoms available. The current work adopts the LLNL alkyl rate constant rule for abstraction by $H\dot{O}_2$ radicals which is higher than the rate constant proposed in ref. [44] by a factor of 1.5. H-atom abstraction by methyl radicals was assumed to be analogous to secondary alkyl abstractions and the current LLNL rate constant rule was applied accounting for available equivalent hydrogen atoms.

Calculations by Al Rashidi et al. [27] were used for the unimolecular decompositions of the cyclopentyl radical and modified based on comparisons to the more recent experimental measurements and high-pressure limit calculations by Manion and Awan [45]. Loss of an H-atom from cyclopentyl was increased by a factor of 1.08, while the ring opening reaction leading to the penten-5-yl radical was increased by a factor of 2.51. The rate constant for cyclopentyl ring opening reaction adopted in this work is very close to the logarithmic average rate between the studies by Al Rashidi et al. and Manion and Awan and is in reasonable agreement given their uncertainties. Additionally, increasing the ring opening rate constant provides much better agreement between simulations and measurements of the species selectivities measured in a shock tube by Manion and Awan [45] and of species concentrations in a jet-stirred reactor [6]. As discussed by Al Rashidi et al. [6], and later Manion and Awan [45], the NTC-like conversion of cyclopentane in the jet-stirred reactor for richer mixtures is very sensitive to the branching ratio of C–C bond scission to C–H bond scission. Given the sensitive nature of jet-stirred reactor

simulations to these pathways, high-accuracy pressure-dependent descriptions reconciling the existing literature may be warranted.

The low temperature pathways resulting from the interaction of cyclopentyl radicals and molecular oxygen were largely taken from the work Al Rashidi et al. [27] after removing the local optimizations, or "tunings," because the tunings were not needed in the present kinetic model to obtain good agreement with the experimental validation data. Calculations by Al Rashidi et al. [27] where typically fit to cover the range of 300 – 1200 K, however for some negligible pathways the fitted rates progress to unphysical values beyond 1200 K. These negligible pathways were removed in the current work to avoid adverse impacts of unphysical rate constants on the computed results and the performance of the numerical solvers. One example of such a pathway is the formation of PT1N4Q5J (4-hydroperoxypent-5-yl-1-ene radical) from cyclopentyl + O_2. At temperatures above 2000 K, the 100 atm rate constant from this channel alone can quickly exceed the high-pressure limit of cyclopentyl + O_2, $\sim 3 \times 10^{12}$ s^{-1}, given in Table 3 of Al Rashidi et al. [27] due to a large exponent, n, in the modified Arrhenius format.

Table 4. Reactions, rate constants, and local optimizations to rate constants of the cyclopentane sub-model in this work. Reactions and/or rate constants which were (a) modified from Al Rashidi et al. [27] or (b) added in this work are marked accordingly. Unmarked reactions were present in the work of Al Rashidi et al. and not modified. Rate constants are presented in the form of $k = AT^n \exp(-E/RT)$ with units of s, mol, cm^3, K, and cal. All rate constants account for appropriate reaction path degeneracies.

Reaction	A	n	E	Reference	Notes

(R1)a	CPT=C_5H_{10}-1	2.45E+20	−0.970	92860.	[36]	
	DUP	1.15E+20	−0.878	92230.	[36]	
(R2)a	CPT=cC_3H_6+C_2H_4	2.14E+24	−1.542	112490.	[36]	c
(R3)	cy$\dot{C}_5H_9$+$\dot{H}$=CPT	1.00E+14	0.000	0	estimate	
(R4)a	CPT+O_2=cy$\dot{C}_5H_9$+$H\dot{O}_2$	9.00E+14	0.000	52904.	estimate	d
(R5)a	CPT+$\dot{H}$=cy$\dot{C}_5H_9$+H_2	1.76E+07	2.000	4600.	[39]	e
(R6)a	CPT+$\ddot{O}$=cy$\dot{C}_5H_9$+$\dot{O}H$	2.89E+05	2.600	2762.	[40]	
(R7)	CPT+$\dot{O}H$=cy$\dot{C}_5H_9$+H_2O	8.37E+07	1.779	−193.	[41]	
(R8)a	CPT+$H\dot{O}_2$=cy$\dot{C}_5H_9$+H_2O_2	4.74E+02	3.370	13719.	[44]	f
(R9)a	CPT+$\dot{C}H_3$=cy$\dot{C}_5H_9$+CH_4	4.20E+05	2.100	7574.	[46]	g
(R10)a	cy$\dot{C}_5H_9$=cyC_5H_8+$\dot{H}$	PLOG, see model			[6, 45]	h
(R11)a	cy$\dot{C}_5H_9$=$\dot{C}_5H_9$1-5	PLOG, see model			[6, 45]	i
(R12)a	cy$\dot{C}_5H_9$+O_2=cyC_5H_8+$H\dot{O}_2$	PLOG, see model			[27]	j
(R13)	cy$\dot{C}_5H_9$+O_2=CPT$\dot{O}_2$J	PLOG, see model			[27]	
(R14)	cy$\dot{C}_5H_9$+O_2=CPT1Q2J	PLOG, see model			[27]	
(R15)	cy$\dot{C}_5H_9$+O_2=CPT1Q3J	PLOG, see model			[27]	
(R16)a	CPT$\dot{O}_2$J=CPT1Q2J	PLOG, see model			[27]	k
(R17)a	CPT$\dot{O}_2$J=CPT1Q3J	PLOG, see model			[27]	k
(R18)	CPT$\dot{O}_2$J=cyC_5H_8+$H\dot{O}_2$	PLOG, see model			[27]	
(R19)	CPT1Q2J=CPTYO12+$\dot{O}H$	PLOG, see model			[27]	
(R20)	CPT1Q3J=CPTYO12+$\dot{O}H$	PLOG, see model			[27]	
(R21)	CPT1Q3J=CPTYO13+$\dot{O}H$	PLOG, see model			[27]	
(R22)	CPT1Q2J=cyC_5H_8+$H\dot{O}_2$	PLOG, see model			[27]	
(R23)	CPT1Q3J=cyC_5H_8+$H\dot{O}_2$	PLOG, see model			[27]	
(R24)	CPT1Q3J=>$\dot{C}_4H_7$CHO-4+$\dot{O}H$	PLOG, see model			[27]	
(R25)	CPT1Q3J=PT1N4Q5J	PLOG, see model			[27]	
(R26)	CPT1Q2J+O_2=CPTQ2QJ	PLOG, see model			[27]	l
(R27)	CPT1Q3J+O_2=CPTQ3QJ	PLOG, see model			[27]	l
(R28)b	CPTQ2QJ=cyC_5E1-3O_2H+$H\dot{O}_2$	PLOG, see model			[27]	m
(R29)b	CPTQ3QJ=cyC_5E1-3O_2H+$H\dot{O}_2$	PLOG, see model			[27]	m
(R30)b	CPTQ3QJ=cyC_5E1-4O_2H+$H\dot{O}_2$	PLOG, see model			[27]	m
(R31)a	CPTQ2QJ=>CPN-2OOH+$\dot{O}H$	PLOG, see model			[27]	n
(R32)a	CPTQ3QJ=>CPN-3OOH+$\dot{O}H$	PLOG, see model			[27]	o
(R33)b	CPTQ3QJ=CPT2Q4Q1J	PLOG, see model			[27]	p
(R34)b	CPT2Q4Q1J=cyC_5E1-4O_2H+$H\dot{O}_2$	PLOG, see model			[27]	q
(R35)b	CPT2Q4Q1J=>C_2H_3C(OO)CCVO+$\dot{O}H$	PLOG, see model			[27]	r
(R36)a	CPN-2OOH=>CO+C_2H_4+$\dot{C}H_2$CHO+$\dot{O}H$	1.50E+16	0.000	43000.	[47, 48]	s
(R37)a	CPN-2OOH=>CH_2CO+$\dot{C}H_2CH_2$CHO+$\dot{O}H$	1.50E+16	0.000	43000.	[47, 48]	s
(R38)a	CPN-3OOH=>C_2H_4+CO+$\dot{C}H_2$CHO+$\dot{O}H$	1.50E+16	0.000	43000.	[47, 48]	s
(R39)a	CPN3OOH=>CH_2CO+$\dot{C}H_2CH_2$CHO+$\dot{O}H$	1.50E+16	0.000	43000.	[47, 48]	s
(R40)a	CPTO_2H+O_2=CPT$\dot{O}_2$J+$H\dot{O}_2$	9.00E+13	0.000	41074.	estimate	d

(R41)a	CPTO$_2$H=CPTÒJ+ÒH	1.50E+16	0.000	43000.	[47, 48]	s
(R42)a	Ċ$_3$H$_5$-a+C$_2$H$_4$=Ċ$_5$H$_9$1-5	PLOG, see model			[49]	

[c] Products were previously propene (C$_3$H$_6$) and ethylene (C$_2$H$_4$).

[d] See main text for discussion of RH + O$_2$ = Ṙ + HȮ$_2$.

[e] The current rate constant is almost an order of magnitude slower than Al Rashidi.

[f] A×1.5 (for the RH + HȮ$_2$ = Ṙ + H$_2$O$_2$ rate constant rule, see main text).

[g] As secondary alkane RH + ĊH$_3$ = Ṙ + CH$_4$ rate constant rule.

[h] A×1.08, see main text for discussion. A typographical error was found in the 1 atm entry activation energy of Al Rashidi and corrected in this work.

[i] A×2.51, see main text for discussion.

[j] A local optimization of –1 kcal/mol to E was removed for this formally direct pathway. H-atom abstraction pathways from the radical by O$_2$ included in Al Rashidi were deemed negligible in this work.

[k] A local optimization of E–0.6 kcal/mol was removed.

[l] Analogy, A×0.5 as R13.

[m] Analogy, A×0.5 for reaction path degeneracy (RPD) as R18.

[n] A×0.25(RPD), E–2 kcal/mol as (R16); previously A×0.5, E–10.1 kcal/mol as (R16).

[o] A×0.25(RPD), E–2 kcal/mol as (R17); previously A×0.5, E–3.7 kcal/mol as (R17).

[p] Analogy, A×0.5 (RPD) as (R17).

[q] Analogy, as (R22).

[r] Analogy, A×0.5 (RPD) as (R11).

[s] A×0.5, estimate based on logarithmic mean of CH$_3$OOH and HOOCH$_2$CH$_2$CHO decomposition rate constants.

3.3 Cyclopentene sub-model

A summary of the reaction pathways and rate constants from the current kinetic sub-model for cyclopentene is presented in Table 5. In addition to the loss of H-atoms, there are two well-known unimolecular decomposition reactions of cyclopentene, which is a major intermediate in the oxidation and pyrolysis of cyclopentane. The first unimolecular reaction is the dehydrogenation to cyclopentadiene and molecular hydrogen, and the current work uses the rate coefficients from Lewis et al. [50]. Manion and Awan [45] also provide the most recent

LLNL-JRNL-811439-DRAFT

assessment of the cyclopentene dehydrogenation reaction which is in good agreement with the value of Lewis et al. [50]. The other unimolecular reaction is the pericyclic formation of vinyl cyclopropane [51], and the current rate constant was adopted from Lewis et al. [52]. It should be noted that vinyl cyclopropane can then further undergo rapid unimolecular isomerization to the linear pentadiene isomers, and the corresponding rates in this study were adopted from Wellington et al. [53]. The rate constant for the termination reaction involving the addition of a $\dot{H}$ atom to a cyclopenten-4-yl radical was estimated to be 1×10^{14} cm^3 mol^{-1} s^{-1}. For the resonance-stabilized cyclopenten-3-yl radical, an estimation was made via analogy to the high-pressure limit calculation by Harding et al. [54] for the termination reaction of a hydrogen atom with an allyl ($\dot{C}_3H_5$-a) radical.

Analogies to the cyclopentane rate constants discussed in Section 3.2 were applied for H-atom abstractions of cyclopentene by small radicals (O$_2$, $\dot{H}$, $\ddot{O}$, $\dot{O}H$, $H\dot{O}_2$, $\dot{C}H_3$) forming the cyclopenten-4-yl radical. H-atom abstractions by $\dot{H}$, $\ddot{O}$, $\dot{O}H$, and $H\dot{O}_2$ leading to the formation of the resonantly stabilized cyclopenten-3-yl radical were estimated by analogy to literature calculations for other C$_3$ – C$_5$ resonance stabilized radicals [55-58]. For H-atom abstraction by O$_2$, the analogous rate constant rule discussed in Section 3.2 was applied with a corrective multiplicative factor of e^{-2} to the pre-exponential factor to account for resonance. As noted by Baulch et al. [59], experiments targeting the C$_3$H$_6$ + O$_2$ = $\dot{C}_3H_5$-a + H$\dot{O}_2$ reaction indicated that the rate constant rule for RH + O$_2$ = $\dot{R}$ + H$\dot{O}_2$ needed a corrective factor to capture the lower rate constant measured. In their 1994 review, Baulch et al. [59] also comment that RH + O$_2$ = $\dot{R}$ + H$\dot{O}_2$ reactions for species such as propene are likely to be slower due to "loss of entropy of activation due to the emerging electron-delocalized allyl radical." This loss of entropy leads to a lower A-factor in their recommendations of an order of magnitude. This pre-exponential factor

correction, e^{-2} (equivalent to dividing by ~7.4), is similar to the effective loss of a single rotor as discussed by Wang et al. [60, 61] for H-atom shift and ring-closure reactions. Several other groups have reported similar trends between pre-exponential factors and hindered rotors for various reactions. This proposed estimation method is compared to recent calculations for RH + $O_2 = \dot{R} + H\dot{O}_2$ reactions with resonance radical products [62] in the supplemental material. Wang et al. [63] calculated the abstraction from cyclopentene by methyl radicals leading to cyclopentene-3-yl radical formation and this rate constant is used in the current work. Abstractions of the vinylic hydrogen from cyclopentene were considered minor pathways and were not included in the current work.

Chemically activated $\dot{H}$ atom addition pathways for cyclopentene were adopted from the calculations of Wang et al. [49]. $\dot{H}$ atom addition to cyclopentene forming cyclopentyl radical is the reverse reaction of cyclopentyl radical decomposition, discussed in Section 3.2. Reactions involving the addition of $\ddot{O}$ and $\dot{C}H_3$ radicals have not been extensively studied for cyclopentene and further studies are warranted. Cyclopentene + $\dot{O}H$ addition was included by analogy to C_3H_6 + $\dot{O}H$ addition [64]. Subsequent O_2 addition leading to Waddington decomposition pathways were also included in the model and presented in Table 5. Cyclopentene + $H\dot{O}_2$ pathways were included in the work of Al Rashidi [27] and retained in this study.

Unimolecular reactions of cyclopentenyl radicals were included using calculations from Wang et al. [49]. While it is known that allylic radical self-recombination reactions [65, 66] occur, the self-recombination of cyclopenten-3-yl radicals has not been studied to the authors' knowledge and therefore this pathway was neglected in the current work. Similarly, limited information is available regarding the reactions of cyclopenten-3-yl radicals with molecular oxygen or hydroxyl radicals, and these pathways were neglected. Reactions of cyclopenten-3-yl

radicals with atomic oxygen were estimated as irreversible reactions using the calculations of Ghildina et al. [67] for the cyclopentadienyl radical system.

A possibly important reaction in the oxidation of cyclopentene is the reaction of cyclopenten-3-yl and $H\dot{O}_2$ radicals. Two sets of products were considered, stabilization to 3-hydroperoxycyclopentene and the chemically activated formation of cyclopenten-3-oxy and hydroxyl radicals. In this work, the rate constants are adopted from the calculations by Goldsmith et al. [68] for the $\dot{C}_3H_5$-a + $H\dot{O}_2$ system. Ring opening of the cyclopentene-3-oxy radical was estimated using the work of Wang et al. [69] and written as a ring closing reaction.

Table 5. Reactions, rate constants, and local optimizations to rate constants of the cyclopentene sub-model in this work. Reactions and/or rate constants which were (a) modified from Al Rashidi et al. [27] or (b) added in this work are marked accordingly. Unmarked reactions were present in the work of Al Rashidi et al. and not modified. Rate constants are presented in the form of $k = AT^n \exp(-E/RT)$ with units of s, mol, cm³, K, and cal. All rate constants account for appropriate reaction path degeneracies.

	reaction	A	n	E	reference	notes
(R1)	$cy\dot{C}_5H_71\text{-}4+\dot{H}=cyC_5H_8$	1.00E+14	0.000	0	estimate	
(R2)a	$cy\dot{C}_5H_71\text{-}3+\dot{H}=cyC_5H_8$	2.00E+14	0.000	0	estimate	
(R3)	$cyC_5H_8=C_5H_6+H_2$	2.24E+13	0.000	60010.	[50]	
(R4)b	$cC_3H_5\text{-}C_2H_3=cyC_5H_8$	2.00E+14	0.000	51670.	[52]	
(R5)a	$cyC_5H_8+O_2=cy\dot{C}_5H_71\text{-}4+H\dot{O}_2$	1.80E+14	0.000	52904.	estimate	c
(R6)a	$cyC_5H_8+\dot{H}=cy\dot{C}_5H_71\text{-}4+H_2$	3.52E+06	2.000	4600.	[39]	d
(R7)a	$cyC_5H_8+\ddot{O}=cy\dot{C}_5H_71\text{-}4+\dot{O}H$	5.78E+04	2.600	2762.	[40]	e
(R8)	$cyC_5H_8+\dot{O}H=cy\dot{C}_5H_71\text{-}4+H_2O$	1.67E+07	1.779	−193.	[41]	f
(R9)a	$cyC_5H_8+H\dot{O}_2=cy\dot{C}_5H_71\text{-}4+H_2O_2$	9.48E+01	3.370	13719.	[44]	g
(R10)a	$cyC_5H_8+\dot{C}H_3=cy\dot{C}_5H_71\text{-}4+CH_4$	8.40E+04	2.100	7574.	[46]	h
(R11)a	$cyC_5H_8+O_2=cy\dot{C}_5H_71\text{-}3+H\dot{O}_2$	4.87E+13	0.000	38974.	estimate	i
(R12)a	$cyC_5H_8+\dot{H}=cy\dot{C}_5H_71\text{-}3+H_2$	1.72E+08	1.847	3337.	[56]	j
(R13)a	$cyC_5H_8+\ddot{O}=cy\dot{C}_5H_71\text{-}3+\dot{O}H$	1.91E+02	3.374	174.	[55]	k
(R14)a	$cyC_5H_8+\dot{O}H=cy\dot{C}_5H_71\text{-}3+H_2O$	4.04E+06	2.200	−437.	[57]	l

(R15)a	$cyC_5H_8+H\dot{O}_2=cy\dot{C}_5H_71\text{-}3+H_2O_2$	7.82E-01	3.968	11702.	[58]	m
(R16)a	$cyC_5H_8+\dot{C}H_3=cy\dot{C}_5H_71\text{-}3+CH_4$	1.72E+03	2.950	5320.	[63]	
(R17)b	$cyC_5H_8+\dot{H}=C_5H_81\text{-}3+\dot{H}$	PLOG, see model			[49]	
(R18)b	$cyC_5H_8+\dot{H}=C_5H_8D14+\dot{H}$	PLOG, see model			[49]	
(R19)b	$cyC_5H_8+\dot{H}=\dot{C}_5H_91\text{-}3$	PLOG, see model			[49]	
(R20)b	$cyC_5H_8+\dot{H}=\dot{C}_5H_91\text{-}4$	PLOG, see model			[49]	
(R21)b	$cyC_5H_8+\dot{H}=\dot{C}_5H_91\text{-}5$	PLOG, see model			[49]	
(R22)b	$cyC_5H_8+\dot{H}=\dot{C}_5H_92\text{-}4$	PLOG, see model			[49]	
(R23)b	$cyC_5H_8+\dot{H}=\dot{C}_5H_92\text{-}5$	PLOG, see model			[49]	
(R24)b	$cyC_5H_8+\dot{H}=\dot{C}_2H_5+C_3H_4\text{-}a$	PLOG, see model			[49]	
(R25)b	$cyC_5H_8+\dot{H}=\dot{C}_2H_5+C_3H_4\text{-}p$	PLOG, see model			[49]	
(R26)b	$cyC_5H_8+\dot{H}=\dot{C}_3H_5\text{-}a+C_2H_4$	PLOG, see model			[49]	
(R27)b	$cyC_5H_8+\dot{H}=\dot{C}_2H_3+C_3H_6$	PLOG, see model			[49]	
(R28)b	$cyC_5H_8+\dot{H}=n\dot{C}_3H_7+C_2H_2$	PLOG, see model			[49]	
(R29)b	$cyC_5H_8+\dot{H}=\dot{C}H_3+C_4H_6$	PLOG, see model			[49]	
(R30)b	$cyC_5H_8+OH=CPTOH\text{-}2$	PLOG, see model			[64]	n
(R31)b	$C_5H_911OH\text{-}5=CPTOH\text{-}2$	1.65E+07	1.020	14200.	[69]	o
(R32)b	$CPTOH\text{-}2+O_2=CPTOH\text{-}2O_2$	9.29E+12	−0.200	−800.	[27]	p
(R33)b	$CPTOH\text{-}2O_2=CPTO_2H\text{-}2\dot{O}$	2.91E+12	−0.226	22300.	[70]	q
(R34)b	$CPTO_2H\text{-}2\dot{O}=>CHOCCCCHO+\dot{O}H$	5.36E+12	−0.080	10790.	[70]	r
(R35)	$cyC_5H_8+H\dot{O}_2=CPTYO12+\dot{O}H$	PLOG, see model			[27]	
(R36)	$cyC_5H_8+H\dot{O}_2=CPTYO13+\dot{O}H$	PLOG, see model			[27]	
(R37)b	$cy\dot{C}_5H_71\text{-}4=cy\dot{C}_5H_71\text{-}3$	PLOG, see model			[49]	
(R38)a	$\dot{C}_5H_714\text{-}1=cy\dot{C}_5H_71\text{-}3$	PLOG, see model			[49]	
(R39)a	$\dot{C}_5H_714\text{-}1=cy\dot{C}_5H_71\text{-}4$	PLOG, see model			[49]	
(R40)a	$\dot{C}VCCVC\dot{C}J= cy\dot{C}_5H_71\text{-}3$	PLOG, see model			[49]	
(R41)a	$\dot{C}VCCVC\dot{C}J= cy\dot{C}_5H_71\text{-}4$	PLOG, see model			[49]	
(R42)b	$cy\dot{C}_5H_71\text{-}3=\dot{C}_2H_3+C_3H_4\text{-}a$	PLOG, see model			[49]	
(R43)b	$cy\dot{C}_5H_71\text{-}3=\dot{C}_3H_5\text{-}a+C_2H_2$	PLOG, see model			[49]	
(R44)b	$cy\dot{C}_5H_71\text{-}4=\dot{C}_3H_5\text{-}a+C_2H_2$	PLOG, see model			[49]	
(R45)b	$cy\dot{C}_5H_71\text{-}4=\dot{C}_2H_3+C_3H_4\text{-}a$	PLOG, see model			[49]	
(R46)b	$cy\dot{C}_5H_71\text{-}3+\dot{O}=>\dot{C}_4H_71\text{-}4+CO$	PLOG, see model			[67]	s
(R47)b	$cy\dot{C}_5H_71\text{-}3+\dot{O}=>CPND2+\dot{H}$	PLOG, see model			[67]	t
(R48)a	$cy\dot{C}_5H_71\text{-}3+H\dot{O}_2=cyC_51EN3\dot{O}J+\dot{O}H$	PLOG, see model			[68]	u
(R49)b	$cy\dot{C}_5H_71\text{-}3+H\dot{O}_2=cyC_5E1\text{-}3O_2H$	PLOG, see model			[68]	v
(R50)b	$cyC_5E1\text{-}3O_2H=cyC_51EN3\dot{O}J+\dot{O}H$	PLOG, see model			[68]	w
(R51)b	$cyC_51EN3\dot{O}J=CPND2+\dot{H}$	3.00E+13	0.000	19078.	[68]	x
(R52)a	$\dot{C}_4H_6CHO2\text{-}5=cyC_51EN3\dot{O}J$	3.06E+11	0.000	10700.	[69]	y
(R53)b	$cyC_51EN3\dot{O}J=CPN\text{-}3R$	3.71E+11	0.000	17534.	[68]	z
(R54)b	$cy\dot{C}_5H_71\text{-}4+O_2=C_5H_6+H\dot{O}_2$	PLOG, see model			[27]	aa
(R55)b	$cy\dot{C}_5H_71\text{-}4+O_2=cyC_5E1\text{-}4\dot{O}_2$	PLOG, see model			[27]	ab

(R56)b	cyC$_5$E1-4$\dot{O}_2$=C$_5$H$_6$+H$\dot{O}_2$	PLOG, see model	[27]	ac

[c] A×2/5 for reaction path degeneracy (RPD) as CPT+O$_2$=cy$\dot{C}_5$H$_9$+H$\dot{O}_2$, see Table 4 of this work. See main text for discussion of RH + O$_2$ = $\dot{R}$ + H$\dot{O}_2$.

[d] A×2/5(RPD) as CPT + $\dot{H}$ = cy$\dot{C}_5$H$_9$ + H$_2$, see Table 4 of this work.

[e] A×2/5(RPD) as CPT + $\ddot{O}$ = cy$\dot{C}_5$H$_9$ + $\dot{O}$H, see Table 4 of this work.

[f] A×2/5(RPD) as CPT + $\dot{O}$H = cy$\dot{C}_5$H$_9$ + H$_2$O, see Table 4 of this work.

[g] A×2/5(RPD) as CPT + H$\dot{O}_2$ = cy$\dot{C}_5$H$_9$ + H$_2$O$_2$, see Table 4 of this work.

[h] A×2/5(RPD) as CPT + $\dot{C}$H$_3$ = cy$\dot{C}_5$H$_9$ + CH$_4$, see Table 4 of this work.

[i] A×exp(–2) to account for resonance stabilized product. See main text for discussion of RH + O$_2$ = $\dot{R}$ + O$_2$.

[j] A×2(RPD) as C$_5$H$_6$ + $\dot{H}$ = $\dot{C}_5$H$_5$ + H$_2$, see Table 6 of this work.

[k] A×4/3(RPD) as C$_3$H$_6$ + $\ddot{O}$ = $\dot{C}_3$H$_5$-a + $\dot{O}$H.

[l] A×2(RPD) as C$_4$H$_8$-1 + $\dot{O}$H = $\dot{C}_4$H$_7$1-3 + H$_2$O.

[m] A×2(RPD) as C$_4$H$_8$-1 + H$\dot{O}_2$ = $\dot{C}_4$H$_7$1-3 + H$_2$O$_2$.

[n] Analogy to C$_3$H$_6$ + $\dot{O}$H = adducts. Note, Al Rashidi lumped directly to products.

[o] Analogy to 1,5-endo ring closure.

[p] As cy$\dot{C}_5$H$_9$+O$_2$ = CPT$\dot{O}_2$J high pressure limit.

[q] As C$_2$C(O[O])CO => C$_2$C(OO)C[O].

[r] As C$_2$C(OO)C[O] => C$_2$H$_5$$\dot{C}$O+CH$_2$O+$\dot{O}$H.

[s] As $\dot{C}_5$H$_5$ + $\ddot{O}$ = C$_4$H$_5$-n + CO.

[t] As $\dot{C}_5$H$_5$ + $\ddot{O}$ = C$_5$H$_4$O + $\dot{H}$.

[u] As $\dot{C}_3$H$_5$-a + H$\dot{O}_2$ = C$_3$H$_5$$\dot{O}$ + $\dot{O}$H.

[v] As $\dot{C}_3$H$_5$-a + H$\dot{O}_2$ = aC$_3$H$_5$OOH.

[w] As aC$_3$H$_5$OOH = C$_3$H$_5$$\dot{O}$+$\dot{O}$H.

[x] As approximate high pressure limit of C$_3$H$_5$$\dot{O}$ = C$_2$H$_3$CHO + $\dot{H}$.

[y] As 1,6-exo ring closure.

[z] A×exp(–2.07) for loss of a rotor as approximate high-pressure limit of C$_3$H$_5$$\dot{O}$ = $\dot{C}$H$_2$CH$_2$CHO.

[aa] As cy$\dot{C}_5$H$_9$ + O$_2$ = cyC$_5$H$_8$ + H$\dot{O}_2$, see Table 4 of this work.

[ab] As cy$\dot{C}_5$H$_9$ + O$_2$ = CPT$\dot{O}_2$J, see Table 4 of this work.

[ac] As CPT$\dot{O}_2$J = cyC$_5$H$_8$ + H$\dot{O}_2$, see Table 4 of this work.

3.4 Cyclopentadiene sub-model

A summary of the reaction pathways and rate constants from the current kinetic sub-model for cyclopentadiene is presented in Table 6. For the unimolecular decomposition of cyclopentadiene, only the loss of a H-atom was considered in this work. The high-pressure limit calculated by Harding et al. [54] was used to write the termination of atomic hydrogen with cyclopentadienyl radicals. H-atom abstractions forming cyclopentadienyl radicals by atomic hydrogen and methyl radicals were modeled using the calculations of Robinson and Lindstedt [56] and Wang et al. [63] respectively. Abstraction by O_2, $\ddot{O}$, $\dot{O}H$, and $H\dot{O}_2$ producing cyclopentadienyl radicals were estimated using the rate constant rule described in Section 3.2 or analogous reactions [55, 57, 58]. Due to the limited number of weak C–H bonds in cyclopentadiene, abstractions from the vinylic sites were considered in this work for their potential importance primarily at high temperature (>1000 K) conditions. Rate constants for the H-atom abstraction by small radicals (O_2, $\dot{H}$, $\ddot{O}$, $\dot{O}H$, $H\dot{O}_2$, $\dot{C}H_3$) leading to vinylic cyclopentadienyl radicals were estimated by a combination of rate constant rules and analogy [71-73].

$\dot{H}$ atom addition to cyclopentadiene, including stabilization and chemically activated pathways, was included in this work using the calculations of Wang et al. [49]. $\ddot{O}$-atom addition to cyclopentadiene forming 1,3-butadiene and carbon monoxide [74] was included using the rate constant for propene and atomic oxygen going to products given by Cavallotti et al. [75]. It should be noted that Nakamura et al. [74] observed additional C_4 products, but we only consider 1,3-butadiene as a lumped C_4 product of $C_5H_6 + \ddot{O}$. Addition reactions of other small radicals ($\dot{O}H$, $H\dot{O}_2$) were not included in this work as the authors are only aware of the proposed rate constants by Zhong and Bozzelli [76] which may not have utilized appropriate methods for

reactions involving resonance stabilized radical pathways. Further studies of these reactions are warranted to understand the low temperature oxidation of cyclopentadiene.

The decomposition of resonance stabilized cyclopentadienyl radicals to either 1-vinylpropargyl, or propargyl and acetylene was considered using the calculations by Da Silva. Several recent computational studies from the Mebel group have been adopted in this work to model the oxidation of cyclopentadienyl radicals by O_2, $\ddot{O}$, and $\dot{O}H$ [67, 77, 78]. Pathways related to methylcyclopentadienes were adopted from Sharma et al. [79] and Dubnikova et al. [80]. Self-recombination of cyclopentadienyl radicals was considered using the rate coefficients given by Cavallotti et al. [65]. For the addition of $H\dot{O}_2$ to cyclopentadienyl radicals, the analogous rate constants for the stabilization and chemically activated products from Goldsmith et al. [68] were used. The rate constants for $H\dot{O}_2$ radical addition were increased by a factor of 2.5 for the number of equivalent resonance sites, and further increased by a factor of two as a local optimization. Unimolecular reactions of the cyclopentadien-5-oxy radical were modeled using the barrier heights from the potential energy surface calculated by Ghildina et al. [67] and pre-exponential factors were estimated. The cyclopentadienyl + $H\dot{O}_2$ reaction and resulting pathways are recommended for further studies due to the conflicting, and often incomplete, nature of current literature.

Table 6. Reactions, rate constants, and local optimizations to rate constants of the cyclopentadiene sub-model in this work. Reactions and/or rate constants which were (a) modified from Al Rashidi et al. [27] or (b) added in this work are marked accordingly. Unmarked reactions were present in the work of Al Rashidi et al. and not modified. Rate constants are presented in the form of $k = AT^n \exp(-E/RT)$ with units of s, mol, cm³, K, and cal. All rate constants account for appropriate reaction path degeneracies.

	Reaction	A	n	E	reference	notes
(R1)a	$\dot{C}_5H_5+\dot{H}=C_5H_6$	3.16E+13	0.281	−179.	[54]	
(R2)a	$C_5H_6+O_2=\dot{C}_5H_5+H\dot{O}_2$	2.44E+13	0.000	37334.	estimate	c
(R3)a	$C_5H_6+\dot{H}=\dot{C}_5H_5+H_2$	8.59E+07	1.847	3337.	[56]	
(R4)a	$C_5H_6+\ddot{O}=\dot{C}_5H_5+\dot{O}H$	9.56E+01	3.374	174.	[55]	d
(R5)a	$C_5H_6+\dot{O}H=\dot{C}_5H_5+H_2O$	2.02E+06	2.200	−437.	[57]	e
(R6)a	$C_5H_6+H\dot{O}_2=\dot{C}_5H_5+H_2O_2$	3.91E-01	3.968	11702.	[58]	f
(R7)a	$C_5H_6+\dot{C}H_3=\dot{C}_5H_5+CH_4$	1.18E+03	2.900	5060.	[63]	
(R8)b	$C_5H_6+O_2=\dot{C}_5H_5\text{-}1+H\dot{O}_2$	1.80E+14	0.000	68874.	estimate	g
(R9)b	$C_5H_6+\dot{H}=\dot{C}_5H_5\text{-}1+H_2$	3.10E+06	2.310	12830.	[22]	h
(R10)b	$C_5H_6+\ddot{O}=\dot{C}_5H_5\text{-}1+\dot{O}H$	7.53E+06	1.910	3736.	[71]	i
(R11)b	$C_5H_6+\dot{O}H=\dot{C}_5H_5\text{-}1+H_2O$	6.75E-02	4.200	860.	[73]	j
(R12)b	$C_5H_6+H\dot{O}_2=\dot{C}_5H_5\text{-}1+H_2O_2$	9.57E+02	3.059	20799.	[22]	k
(R13)b	$C_5H_6+\dot{C}H_3=\dot{C}_5H_5\text{-}1+CH_4$	4.88E+02	2.947	15148.	[72]	l
	DUP	8.13E-05	4.417	8836.	[72]	
(R14)b	$C_5H_6+O_2=\dot{C}_5H_5\text{-}2+H\dot{O}_2$	1.80E+14	0.	68874.	estimate	g
(R15)b	$C_5H_6+\dot{H}=\dot{C}_5H_5\text{-}2+H_2$	3.10E+06	2.31	12830.	[22]	h
(R16)b	$C_5H_6+\ddot{O}=\dot{C}_5H_5\text{-}2+\dot{O}H$	7.53E+06	1.91	3736.	[71]	i
(R17)b	$C_5H_6+\dot{O}H=\dot{C}_5H_5\text{-}2+H_2O$	6.75E-02	4.2	860.	[73]	j
(R18)b	$C_5H_6+H\dot{O}_2=\dot{C}_5H_5\text{-}2+H_2O_2$	9.57E+02	3.059	20799.	[22]	k
(R19)b	$C_5H_6+\dot{C}H_3=\dot{C}_5H_5\text{-}2+CH_4$	4.88E+02	2.947	15148.	[72]	l
	DUP	8.13E-05	4.417	8836.	[72]	
(R20)a	$C_5H_6+\dot{H}=cy\dot{C}_5H_7\text{1-3}$	PLOG, see model			[49]	
(R21)a	$C_5H_6+\dot{H}=cy\dot{C}_5H_7\text{1-4}$	PLOG, see model			[49]	
(R22)a	$C_5H_6+\dot{H}=CVCCVC\dot{C}J$	PLOG, see model			[49]	
(R23)a	$C_5H_6+\dot{H}=\dot{C}_3H_5\text{-a}+C_2H_2$	PLOG, see model			[49]	
(R24)b	$C_5H_6+\dot{H}=C_3H_4\text{-a}+\dot{C}_2H_3$	PLOG, see model			[49]	
(R25)b	$C_5H_6+\ddot{O}=>C_4H_6+CO$	3.45E+09	1.144	0.	[74, 75]	m
(R26)b	$C\#CCVC\dot{C}J=\dot{C}_5H_5$	1.84E+94	−24.400	79300.	[81]	
(R27)a	$\dot{C}_3H_3+C_2H_2=\dot{C}_5H_5$	PLOG, see model			[81]	
(R28)b	$\dot{C}_3H_3+C_2H_2=C\#CCVC\dot{C}J$	PLOG, see model			[81]	
(R29)b	$C\#CCVC\dot{C}J+O_2=C_2H_3CHCO+H\dot{C}O$	1.70E+05	1.700	1500.	[82]	n
(R30)b	$C\#CCVC\dot{C}J+HO_2=>\dot{C}_4H_3\text{-c}+CH_2O+\dot{O}H$	PLOG, see model			[68]	o
(R31)a	$\dot{C}_5H_5+\ddot{O}=\dot{C}_4H_5\text{-n}+CO$	PLOG, see model			[67]	
(R32)a	$\dot{C}_5H_5+\ddot{O}=C_5H_4O+\dot{H}$	PLOG, see model			[67]	
(R33)b	$cyC_5ODEJ=CPND2\text{-4R}$	PLOG, see model			[67]	
(R34)b	$cyC_5ODEJ=CPND2\text{-5R}$	PLOG, see model			[67]	
(R35)b	$cyC_5ODEJ=\dot{C}_5H_4OH$	PLOG, see model			[67]	
(R36)b	$cyC_5ODEJ=C_5H_4\dot{O}+\dot{H}$	PLOG, see model			[67]	
(R37)b	$cyC_5ODEJ=\dot{C}_4H_5\text{-n}+CO$	PLOG, see model			[67]	
(R38)a	$\dot{C}_5H_5+\dot{O}H=C_5H_5OH$	PLOG, see model			[77]	

(R39)b	$\dot{C}_5H_5+\dot{O}H=C_5H_5OH\text{-}1$	PLOG, see model			[77]	
(R40)b	$\dot{C}_5H_5+\dot{O}H=C_5H_5OH\text{-}2$	PLOG, see model			[77]	
(R41)b	$C_5H_5OH=C_5H_5OH\text{-}1$	PLOG, see model			[77]	
(R42)b	$C_5H_5OH=C_5H_5OH\text{-}2$	PLOG, see model			[77]	
(R43)b	$C_5H_5OH\text{-}1=C_5H_5OH\text{-}2$	PLOG, see model			[77]	
(R44)a	$\dot{C}_5H_5+\dot{O}H=C_4H_6+CO$	PLOG, see model			[77]	
(R45)b	$\dot{C}_5H_5+\dot{O}H=CPND2\text{-}4R+\dot{H}$	PLOG, see model			[77]	
(R46)a	$\dot{C}_5H_5+\dot{O}H=\dot{C}_5H_4OH+\dot{H}$	PLOG, see model			[77]	
(R47)b	$\dot{C}_5H_5+\dot{O}H=CPND2\text{-}5R+\dot{H}$	PLOG, see model			[77]	
(R48)b	$C_5H_5OH=C_4H_6+CO$	PLOG, see model			[77]	
(R49)b	$C_5H_5OH\text{-}1=C_4H_6+CO$	PLOG, see model			[77]	
(R50)b	$C_5H_5OH\text{-}2=C_4H_6+CO$	PLOG, see model			[77]	
(R51)b	$C_5H_5OH=CPND2\text{-}4R+\dot{H}$	PLOG, see model			[77]	
(R52)b	$C_5H_5OH\text{-}1=CPND2\text{-}4R+\dot{H}$	PLOG, see model			[77]	
(R53)b	$C_5H_5OH\text{-}2=CPND2\text{-}4R+\dot{H}$	PLOG, see model			[77]	
(R54)a	$C_5H_5OH=\dot{C}_5H_4OH+\dot{H}$	PLOG, see model			[77]	
(R55)b	$C_5H_5OH\text{-}1=\dot{C}_5H_4OH+\dot{H}$	PLOG, see model			[77]	
(R56)b	$C_5H_5OH\text{-}2=\dot{C}_5H_4OH+\dot{H}$	PLOG, see model			[77]	
(R57)b	$C_5H_5OH=CPND2\text{-}5R+\dot{H}$	PLOG, see model			[77]	
(R58)b	$C_5H_5OH\text{-}1=CPND2\text{-}5R+\dot{H}$	PLOG, see model			[77]	
(R59)b	$C_5H_5OH\text{-}2=CPND2\text{-}5R+\dot{H}$	PLOG, see model			[77]	
(R60)b	$\dot{C}_5H_4OH=>C_5H_4O+\dot{H}$	PLOG, see model			[67]	
(R61)b	$C_5H_4O+\dot{H}=>\dot{C}_5H_4OH$	PLOG, see model			[67]	
(R62)b	$C_5H_4OH=\dot{C}_4H_5\text{-}n+CO$	PLOG, see model			[67]	
(R63)b	$\dot{C}_5H_4OH=CPND2\text{-}4R$	PLOG, see model			[67]	
(R64)a	$\dot{C}_5H_5+H\dot{O}_2=C_5H_5\dot{O}+\dot{O}H$	PLOG, see model			[68]	p
(R65)b	$\dot{C}_5H_5+H\dot{O}_2=C_5H_5OOH$	PLOG, see model			[68]	q
(R66)b	$C_5H_5OOH=C_5H_5\dot{O}+\dot{O}H$	PLOG, see model			[68]	r
(R67)b	$C_5H_5\dot{O}=CPND2\text{-}4R$	4.79E+12	0.000	10187.	[61, 67]	s
(R68)a	$\dot{C}JVCCVCCVO=C_5H_5\dot{O}$	3.71E+10	0.000	11287.	[67, 69]	t
(R69)a	$\dot{C}JVCCVCCVO=C_5Y1D24\text{-}1R$	2.62E+10	0.000	8187.	[61, 67]	u
(R70)b	$\dot{C}_5H_5+O_2=>C_5H_5O\dot{O}$	PLOG, see model			[78]	
(R71)b	$C_5H_5O\dot{O}=>\dot{C}_5H_5+O_2$	PLOG, see model			[78]	
(R72)b	$\dot{C}_5H_5+O_2=C_5H_4O+\dot{O}H$	8.77E+01	3.110	23496.	[78]	
(R73)b	$\dot{C}_5H_5+O_2=\dot{C}H_2CHCHCHO+CO$	PLOG, see model			[78]	
(R74)a	$\dot{C}_5H_5+O_2=C_2H_3CHCO+H\dot{C}O$	PLOG, see model			[78]	
(R75)b	$\dot{C}_5H_5+O_2=>H\dot{C}O+\dot{C}JVCCVCVO+\dot{H}$	PLOG, see model			[78]	v
(R76)b	$\dot{C}_5H_5+O_2=C_5H_5\dot{O}+\dot{O}$	PLOG, see model			[78]	
(R77)b	$\dot{C}_5H_5\text{-}1+O_2=CPND2\text{-}4R+\dot{O}$	PLOG, see model			[83]	w
(R78)b	$\dot{C}_5H_5\text{-}2+O_2=CPND2\text{-}5R+\dot{O}$	PLOG, see model			[83]	x

[c] $A \times \exp(-2)$ to account for resonance stabilized product. See main text for discussion of $RH + O_2 = \dot{R} + O_2$.

[d] $A \times 2/3$ for reaction path degeneracy (RPD) as $C_3H_6 + \ddot{O} = \dot{C}_3H_5\text{-a} + \dot{O}H$.

[e] As $C_4H_8\text{-}1 + \dot{O}H = \dot{C}_4H_71\text{-}3 + H_2O$.

[f] As $C_4H_8\text{-}1 + H\dot{O}_2 = \dot{C}_4H_71\text{-}3 + H_2O_2$.

[g] See main text for discussion of $RH + O_2 = \dot{R} + O_2$.

[h] $A \times 0.5$(RPD) as $C_2H_4 + \dot{H} = \dot{C}_2H_3 + H_2$.

[i] $A \times 0.5$(RPD) as $C_2H_4 + \ddot{O} = \dot{C}_2H_3 + \dot{O}H$.

[j] $A \times 0.5$(RPD) as $C_2H_4 + \dot{O}H = \dot{C}_2H_3 + H_2O$.

[k] As $C_3H_6 + HO_2 = \dot{C}_3H_5\text{-s} + H_2O_2$.

[l] $A \times 0.5$(RPD) as $C_2H_4 + \dot{C}H_3 = \dot{C}_2H_3 + CH_4$.

[m] As $C_3H_6 + \ddot{O} = $ products. C4 products described in Nakamura lumped as 1,3-butadiene.

[n] As $\dot{C}_3H_3 + O_2 = CH_2CO + H\dot{C}O$.

[o] As $\dot{C}_3H_5\text{-a} + H\dot{O}_2 = C_3H_5\dot{O} + \dot{O}H$.

[p] $A \times 2.5$(RPD)*2 as $\dot{C}_3H_5\text{-a} + H\dot{O}_2 = C_3H_5\dot{O} + \dot{O}H$.

[q] $A \times 2.5$(RPD)*2 as $\dot{C}_3H_5\text{-a} + H\dot{O}_2 = aC_3H_5OOH$.

[r] As $aC_3H_5OOH = C_3H_5\dot{O} + \dot{O}H$.

[s] Estimated as 1,2 H-shift from Wang. E from potential energy surface of Ghildina.

[t] Estimated as 1,6-exo ring closure with additional hindered rotor correction, $A \times \exp(-2.11)$, from Wang. E from potential energy surface of Ghildina.

[u] $A \times 2$ estimated as 1,5 H-shift with additional hindered rotor correction, $A \times \exp(-2.07)$, from Wang. E from potential energy surface of Ghildina.

[v] $\dot{C}_5H_5 + O_2 = P4$, P4 from Oleinikov assumed to be $H\dot{C}O + \dot{C}JVCCVCVO$.

[w] As $C_5H_3\dot{O}\text{-}3 + O_2 = C_5H_3O\text{-}3\dot{O} + \ddot{O}$.

[x] As $C_5H_3\dot{O}\text{-}3 + O_2 = C_5H_3O\text{-}3\dot{O} + \ddot{O}$.

3.5 Dimethyl ether sub-model

The dimethyl ether sub-model was developed based on the recent study of ethanol and dimethyl ether binary blends by Zhang et al. [20]. Zhang et al. modified the rate constant for carbonyl hydroperoxide ($HC(O)OCH_2OOH$) decomposition to $A = 2.5 \times 10^{16}$ s^{-1} with an $Ea = 43$

kcal mol^{-1} to achieve better modeling agreement with their experiments of ethanol/DME mixtures. This modification was adopted in the current kinetic model.

4. Results and Discussion

The IDT measurements of the binary mixtures investigated during this study were carried out in two independent experimental facilities at NUIG. The relatively fast IDTs (0.06 ~ 6 ms) were carried out in a HPST and the slower IDT (3 ~ 300 ms) measurements in an RCM. Representative experimental and simulated pressure profiles of the CPT/DME blends are shown in Fig. 1 at 20 bar and 40 bar. The experimental IDT data and the volume profiles in a Chemkin input format for all conditions studied are available as Supplementary Material. As depicted in Fig. 1, the model developed in the current study can well reproduce the overall IDT measurements and adequately captures the associated heat release measured experimentally at all conditions investigated (plots attached as Supplementary Material). The heat release manifests itself as a pressure increase due the reacting fuel-air mixture relative to the non-reactive pressure history. In Fig. 1, it is interesting to note the lack of significant heat release measured in the 70/30 CPT/DME experiments prior to ignition and this will be discussed later as it relates to the ignition delay results.
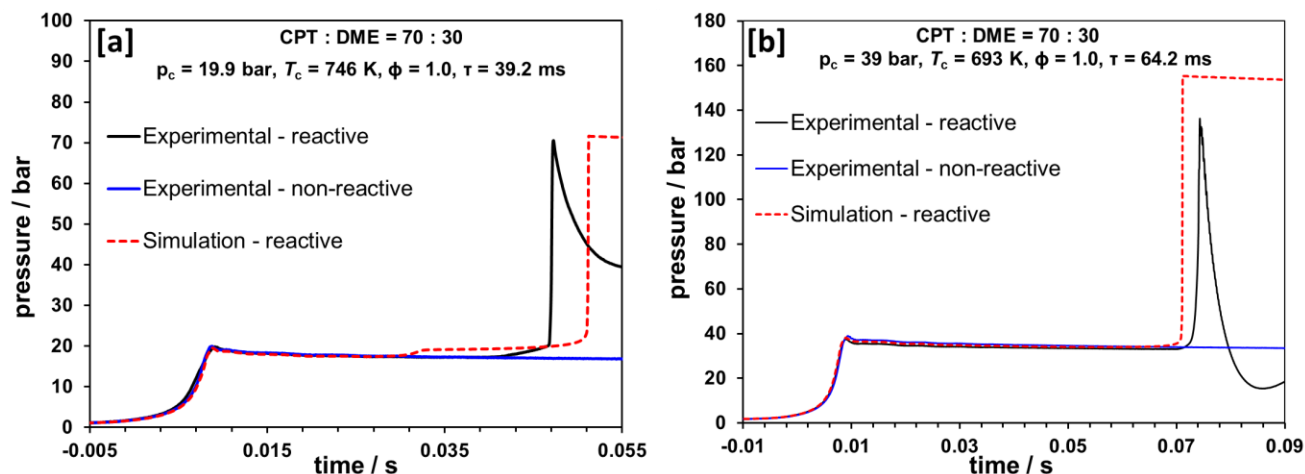
Fig. 1: Representative experimental and simulated pressure profiles of 70CPT/30DME at Φ = 1.0 in air, a) 20 and b) 40 bar using the current kinetic model.

Over the entire range of conditions and mixtures overall IDT are well reproduced by the current model, as shown in the Figs. 2(a) – (f), with simulations typically within 50% of the experimental measurements. The trends of pressure and equivalence ratio on the binary fuel reactivity are provided as Supplemental material. In addition to the current model validation against IDT of neat and DME doped mixtures, the available laminar burning velocity (LBV) measurements from Davis et al. [10], Zhao et al. [11] and speciation data from Al Rashidi et al. [6] and Herbinet et al. [84] were also simulated and presented in the Supplemental material. The current model performance against the auto-ignition data available in the literature for neat DME [85], cyclopentane [12-14] and cyclopentene [86] are also available as Supplementary material.

As with most other hydrocarbon fuels, elevated pressures lead to enhanced reactivity for all mixtures at all temperatures since reaction rates are directly dependent on the absolute concentration of the reactants. Regarding trends in equivalence ratios, the IDTs for all blends exhibit a strong sensitivity to the mixture stoichiometry in the negative temperature coefficient

(NTC) regime. This trend can be understood by noting that the mixture equivalence ratios were controlled by keeping the nominal oxygen concentration constant while varying the fuel concentration. Therefore, for leaner mixtures the amount of reactive DME (and CPT) was reduced in both binary blends at fuel-lean equivalence ratios, limiting the amount of chain-branching low temperature chemistry.
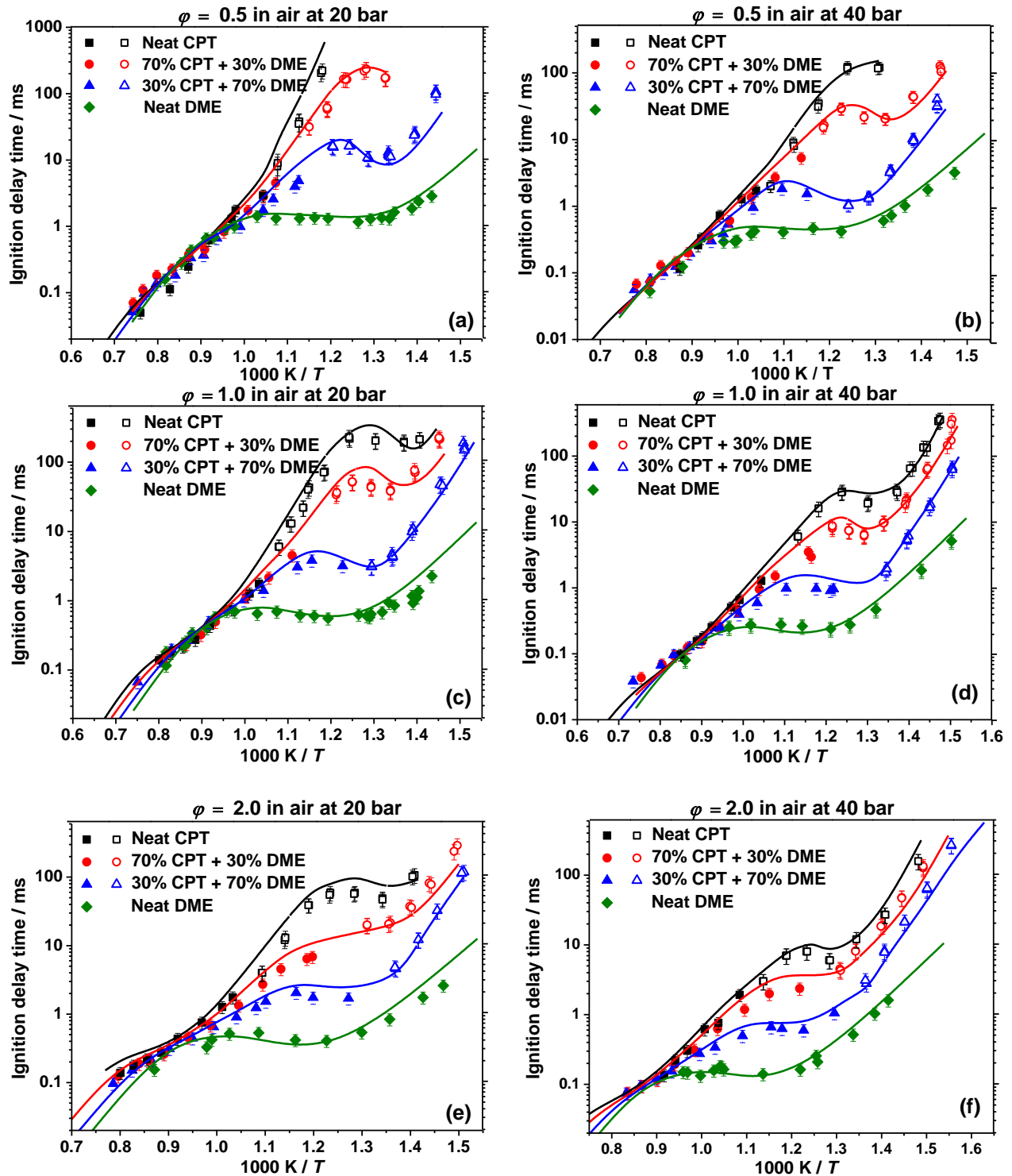
Fig. 2: Influence of doping DME on the reactivity of CPT and comparisons to the model developed in this work. Solid and open symbols correspond to HPST and RCM measurements,

respectively. The binary CPT/DME blends compared were measured as part of this study. Neat CPT and DME measurements are shown from refs. [7], [87], and [88].

Despite the strong non-Arrhenius or even negative temperature coefficient (NTC) behavior in Fig. 2, there is limited low temperature heat release (LTHR) associated with first stage ignition. For most alkanes, non-Arrhenius plots of IDTs are indicators of chain-branching low temperature chemistry which typically manifests itself as two-stage ignition. For mixtures with higher concentrations of CPT at all conditions, the experimental measurements show there is very limited LTHR. Furthermore, when LTHR does occur, it is very close to the overall ignition event, which agrees well with the observations of Fridlyand et al. [15]. The experimental pressure profiles for higher CPT mixtures along with the model simulation are attached in the Supplementary Material. These measurements suggest that CPT oxidation proceeds through low temperature pathways that are not as net exothermic as acyclic alkanes. When CPT is blended with DME, any $\dot{O}H$ radicals from the chain branching reactions of DME are scavenged thereby suppressing LTHR and chain branching. However, for the fuel-lean mixtures with higher DME concentrations, measurable LTHR was observed and is well captured by the model.

Due to the unusual behavior of mixtures with high concentrations of cyclopentane, the reactions controlling the low temperature heat release were investigated for the 70/30 CPT/DME mixture at 750 K and 20 bar. Low temperature exothermicity in the high cyclopentane concentration simulations is primarily derived from addition of cyclopentyl radicals to O_2 (with ~22% exothermicity), analogous to the important low temperature heat release reactions for alkyl mixtures. Additional, but less significant exothermic contributions, stem from H-atom abstraction ($CPT + \dot{O}H = cy\dot{C}_5H_9 + H_2O$ and $H\dot{O}_2 + H\dot{O}_2 = H_2O_2 + O_2$) reactions, among others. Competitive endothermic reactions include the concerted elimination of $H\dot{O}_2$ from cyclopentyl

peroxy radicals (~20% endothermicity). The combined RO–OH bond breaking of 3-hydroperoxycyclopent-1-ene and hydroperoxymethyl formate account for less than 18% of the simulated endothermicity. In this system it is likely the concerted elimination reaction is important as a primary source of $H\dot{O}_2$ radical generation and for endothermicity that suppresses LTHR. The following analysis primarily focuses on the influence of DME doping on the low temperature reactivity of CPT.

4.1 Effect of DME addition on CPT reactivity

The reactivity of CPT is significantly enhanced with the addition of DME at low temperatures (650 – 850 K) as depicted in Fig. 2 for all pressures. For example, in Fig. 2(c) at 750 K the 30% DME mixture increases the reactivity by a factor of five and the 70% DME mixture by approximately two orders of magnitude relative to neat CPT mixtures. To kinetically interpret the observed CPT/DME trends, a flux analyses at $\varphi = 1.0$, $p = 20$ bar and $T = 725$ K is presented in Fig. 3 and the molar consumption yields are expressed in relative amounts. For all mixtures, the CPT chemistry is initiated by H-atom abstraction, primarily by $\dot{O}H$ and $H\dot{O}_2$ radicals, generating cyclopentyl ($cy\dot{C}_5H_9$) radicals. However, as the DME concentration increases in the binary blends, CPT scavenges $\dot{O}H$ radicals that are generated from the DME low temperature chain-branching pathways, Fig. 3. This scavenging is in part due to the number of H-atoms in CPT (10) compared to DME (6) and the relatively limited production of $\dot{O}H$ from neat cyclopentane. CPT does possess a larger C–H bond dissociation enthalpy (BDE) than DME by ~3 kcal mol^{-1}. This is not significantly greater than uncertainties commonly cited in BDE determinations (1~2 kcal/mol). Further, H-atom abstraction rate constants by $\dot{O}H$ radicals tend to be relatively insensitive to BDE changes of only a few kcal or less. For this discussion, enthalpies of reaction (ΔHrxn) of RH + $\dot{O}H$ = $\dot{R}$ + H$_2$O convey the same relative information as

BDE from the components of interest. A figure in the supplemental material presents transition state barrier heights as a function of ΔHrxn for many literature calculations of RH + $\dot{O}$H = $\dot{R}$ + H$_2$O reactions spanning strong C–H bonds (as in acetylene or ethylene) to weak C–H bonds (such as in toluene C$_6$H$_5$CH$_2$–H, or acetaldehyde CH$_3$CO–H). A linear regression of the data, excluding the very strong acetylene C–H datum, illustrates that ΔHrxn is not a strong predictor of barrier height. A difference of 3 kcal/mol would only yield a $0.3 - 0.6$ kcal/mol difference in barrier height and, assuming the activation energy is similarly impacted, potentially change a rate constant at 1000 K by a factor 1.3. In this work, the rate constants for H-atom abstraction by $\dot{O}$H radicals for CPT are within a factor of 1.3 of those for abstraction from DME on a per H-atom basis. This ratio may be higher, or lower, depending on the accuracy of the rate constants implemented in this work. Differences in the number of hydrogen atoms contribute to the apparent scavenging of one species relative to another particularly when the rate constants on a per H basis are similar, as in this study.

After addition of cyclopentyl radicals to O$_2$, the branching ratio of the cyclopentyl peroxy (CPT$\dot{O}_2$J) radical is critical in accurately simulating all mixtures containing CPT. The concerted elimination of H$\dot{O}_2$ from CPT$\dot{O}_2$j radicals forming cyclopentene (cyC$_5$H$_8$) and H$\dot{O}_2$ (R1) dominates for both neat CPT and its mixtures with DME.

$$CPT\dot{O}_2J = cyC_5H_8 + H\dot{O}_2 \hspace{3cm} (R1)$$

Measurements of cyclopentane oxidation in the Orleans jet-stirred reactor from Al Rashidi et al. [6] also support the significance of cyclopentene as an intermediate at temperatures below 1000 K. Unlike linear or branched alkanes, the six-membered 1,5 R$\dot{O}_2$ radical isomerization is hindered due to relatively high ring-strain energy in CPT. According to theoretical calculations of the cyclopentyl peroxy radical reactions by both Miyoshi [89] and Al Rashidi et al. [27],

barrier heights for the concerted elimination are lower (28.2 vs. 30.8 kcal mol^{-1}) than acyclic alkanes. However, barrier heights are significantly higher (25.1 vs. 20.8 kcal mol^{-1}) for 1,5 R$\dot{O}_2$ radical isomerization reactions. This change in branching ratio in favor of higher H$\dot{O}_2$ radical production over R$\dot{O}_2$ radical isomerization and subsequent chain branching largely explains the overall low reactivity of cyclopentane relative to its acyclic counterparts at low temperatures.
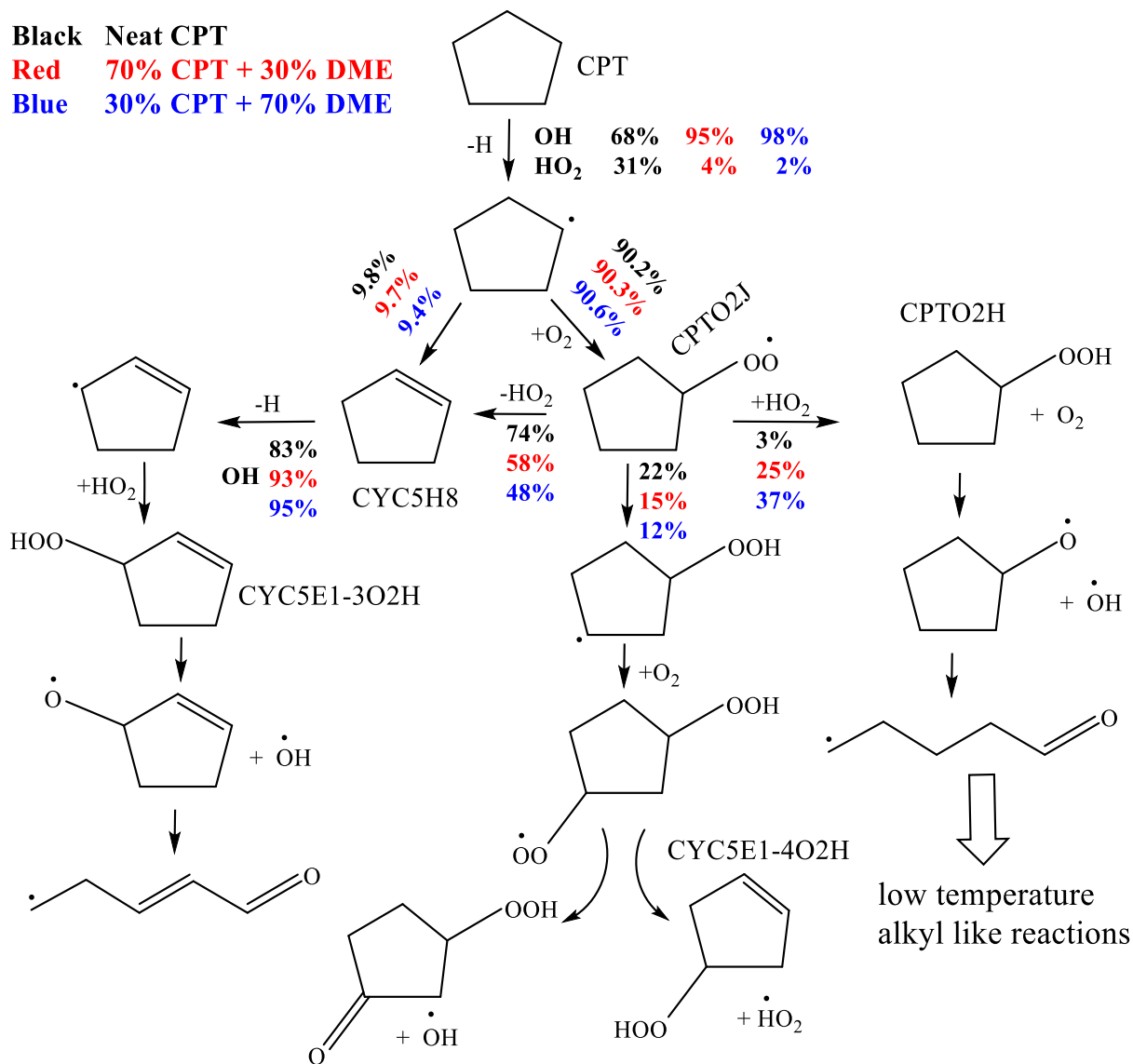

Fig. 3: Flux analysis at 20% fuel consumption and $\varphi = 1.0$, $p = 20$ bar, $T = 725$ K in air for neat CPT and two binary blends with DME using the kinetic model developed in this work.

The relatively large concentration of $H\dot{O}_2$ radicals generated from concerted elimination reactions at low and intermediate temperatures (< 1000 K) contribute to H-atom abstractions of neat CPT mixtures. However, the flux of the concerted elimination channel decreases from 74% for neat CPT to 48% for 30/70 CPT/DME mixtures, respectively. This is due to the increased production of $\dot{O}H$ and the onset of a competing $H\dot{O}_2$ reaction with $CPT\dot{O}_2J$ (R2) in the binary mixtures. Formation of hydroperoxycyclopentane ($CPTO_2H$) for these mixtures is the reverse reaction of H-atom abstraction by O_2 at the hydroxyl site from $CPTO_2H$. This pathway, R2, accounts for 3 – 37% of the consumption of $CPT\dot{O}_2J$ as the concentration of DME increases in each mixture.

$$CPT\dot{O}_2J + H\dot{O}_2 = CPTO_2H + O_2 \qquad\qquad (R2)$$

$$\dot{H} + O_2\ (+M) = H\dot{O}_2\ (+M) \qquad\qquad (R3)$$
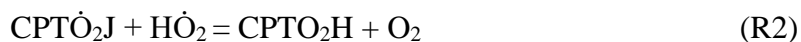
At first this trend might appear counter intuitive. In neat mixtures of DME, 58% of $H\dot{O}_2$ production is from addition of $\dot{H}$ to O_2 (R3) while in neat mixtures of CPT this pathway accounts for less than 1% of $H\dot{O}_2$ production. As the concentration of DME increases for these binary mixtures, the source of $H\dot{O}_2$ radicals shifts from R1 (accounting for 54% of $H\dot{O}_2$ production for neat CPT) to R3. At the same time, the production of $\dot{O}H$ radical increases due to the low temperature DME chain-branching pathways. Since H-abstraction by $\dot{O}H$ is faster than by $H\dot{O}_2$, CPT scavenges the $\dot{O}H$ radicals generated from DME leaving $H\dot{O}_2$ to react with other species such as the $CPT\dot{O}_2J$ radical as shown in Fig 3. The influence of R2 on IDT predictions is depicted in Figs. 4(a) and 4(b) for φ = 1.0 in air at 20 bar and 40 bar, respectively. For the conditions of this study, this pathway has a significant effect on the neat CPT and 70/30 CPT/DME mixtures because the product from ring-opening of the cyclopentoxy radical in Fig. 3

LLNL-JRNL-811439-DRAFT

promotes low temperature chain branching. When the concentration of CPT is further reduced in mixtures, the simulations are controlled by the DME chain-branching pathways. Considering the sensitivity of R2, further theoretical and/or experimental studies are warranted of this pathway and its products.
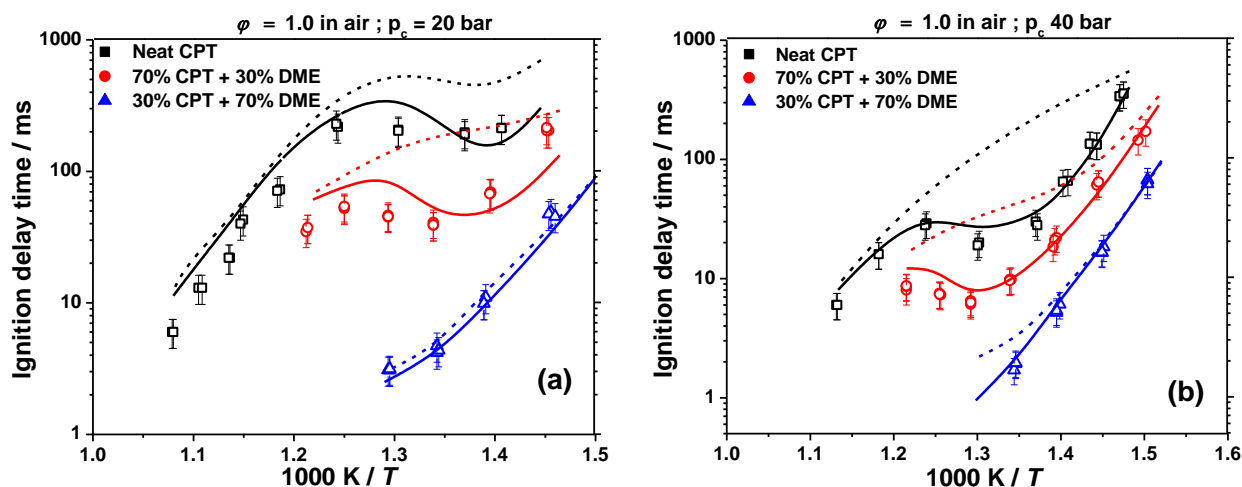

Fig. 4: Influence of R2, $CPT\dot{O}_2J + H\dot{O}_2 = CPTO_2H + O_2$, when included (solid) and excluded (dashed), on the current model performance of neat and DME doped CPT.

$H\dot{O}_2$ radicals can also add to the resonance stabilized radicals produced from cyclopentene, leading to the production of adducts for all mixtures as shown in Fig. 3. These adducts eventually undergo RO–OH bond scission and subsequent ring opening. At high temperatures, resonance stabilized radicals can consume $H\dot{O}_2$ radicals through chemically activated pathways producing reactive hydroxyl and allyloxy radicals. Either reaction sequence converts the abundant and less reactive $H\dot{O}_2$ radicals produced from CPT oxidation to relatively more reactive $\dot{O}H$ radicals.

At higher temperatures (> 1000 K) the experimental measurements of the neat and blended fuels exhibit similar reactivities, Fig. 2. To further analyze this trend in reactivity, the fuel oxidation scheme for the major pathways at $T = 1100$ K, $p = 20$ bar, $\varphi = 1.0$ and 20% fuel

consumption is provided in Fig. 5. The oxidation of CPT at high temperatures is also initiated by H-atom abstraction by $\dot{O}H$, $H\dot{O}_2$, and $\dot{H}$ radicals which account for 65%, 20%, and 10% respectively of the fuel flux. Approximately 55% of cyclopentyl radicals undergo β-scission to yield $cyC_5H_8 + \dot{H}$ while 35% of cyclopentyl radicals undergo ring opening to form linear pent-1-en-5-yl radicals via C–C bond cleavage. Subsequently, pent-1-en-5-yl radicals undergo β-scission to form ethylene (C_2H_4) and $\dot{C}_3H_5$-a radicals. The major consumption pathway of cyC_5H_8 is through H-atom abstraction at the allylic sites and is followed by β-scission to form cyclopentadiene (C_5H_6). The remaining cyclopentyl radicals, ~10%, are converted to $CPT\dot{O}_2J$ which ultimately forms cyC_5H_8 via concerted elimination of $H\dot{O}_2$ radicals.

LLNL-JRNL-811439-DRAFT
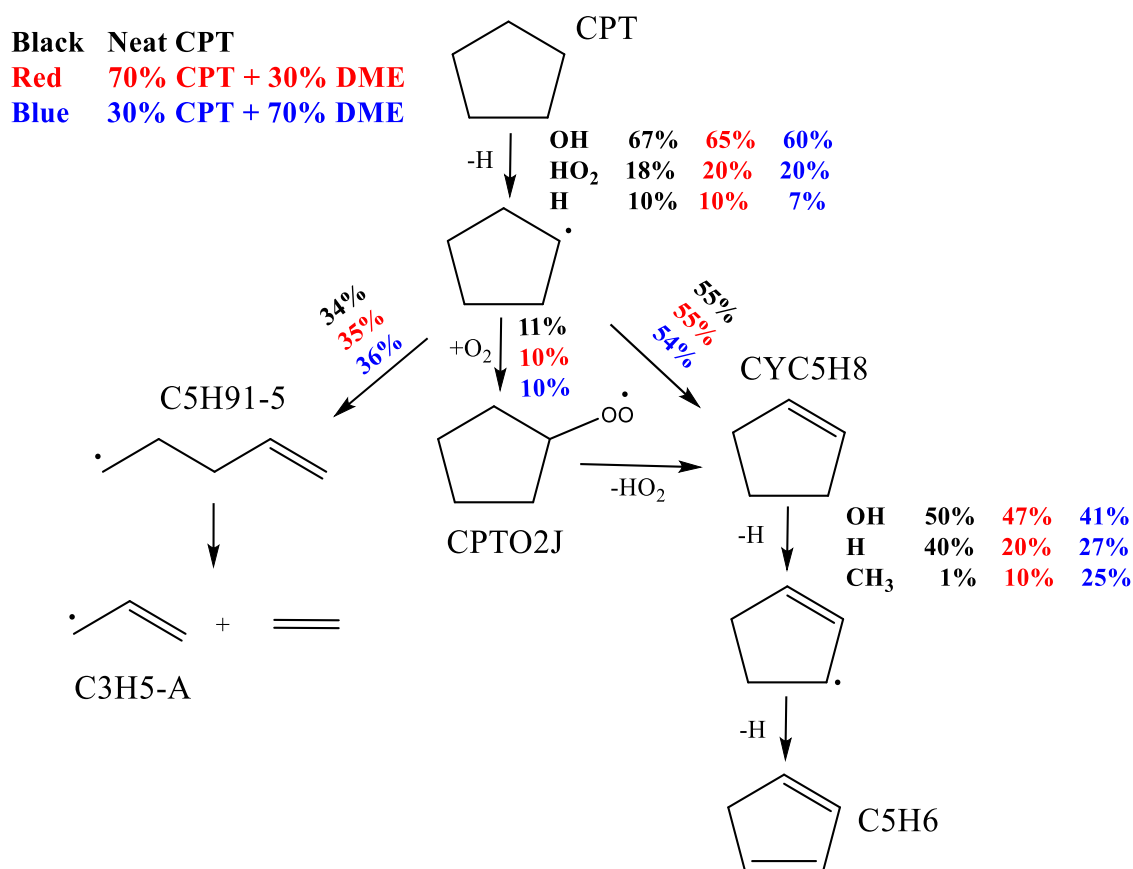
Fig. 5: Flux analyses at 20% fuel consumption and $\varphi = 1.0$, 20 bar, 1100 K in air for neat CPT and two binary blends with DME using the kinetic model developed in this work.

4.2 Blending slopes with DME addition

Two recent studies have considered binary blends of DME with ethanol and toluene, both relatively unreactive fuels at low temperatures. These studies provide additional context for the current IDT measurements of CPT/DME mixtures. Figure 6 compares the reactivity trends for CPT, ethanol and toluene mixtures with increasing fractions of DME for $\varphi = 1.0$, 20 bar at three temperatures using kinetic models from this study and ref. [19], and [20] respectively.
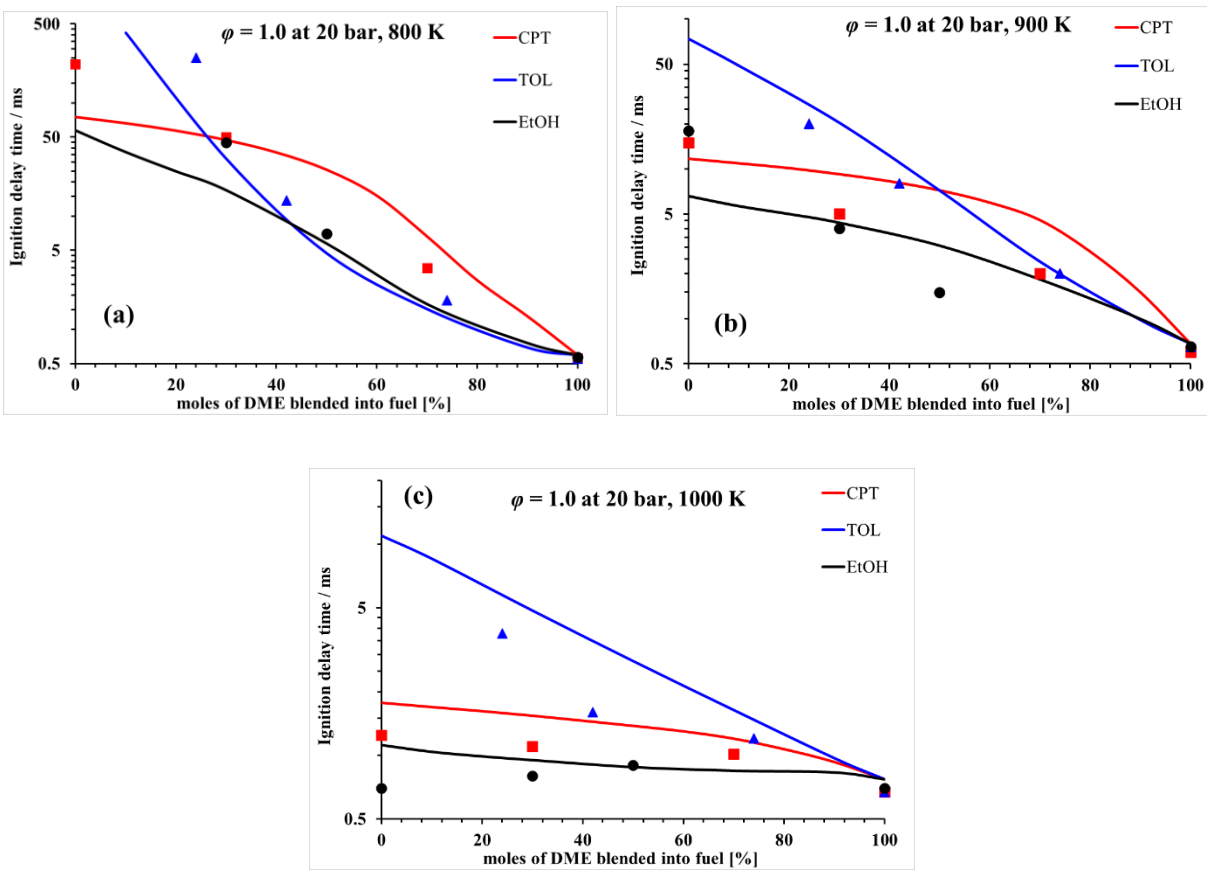
Fig. 6 The experimental data (ST/RCM) and constant volume simulations representing the reactivity trends of CPT, ethanol, and toluene kinetic models with DME addition at $\varphi = 1.0$ in air, 20 bar and $800 - 1000$ K.

The blending slopes of the three fuels are relatively insensitive to DME addition at temperatures ≥ 1100 K. However, adding DME increases the reactivity of all fuels (CPT, ethanol, and toluene) with the effect being strongest at low temperatures (≤ 900 K). Compared to ethanol and toluene blends, the blending slope of CPT in Fig. 6 is not significantly perturbed until more than 50% molar DME addition at all temperatures, since CPT chemistry has both low temperature chain branching and propagation pathways. With 20% DME addition to the fuel, the blending slope of toluene is steepest followed by ethanol and CPT at all temperatures in Fig. 6.

This ordering can be explained by following the flux of the respective fuel radicals at 800 K. In the case of CPT and ethanol, there is significant generation of chain propagating $H\dot{O}_2$ radicals via major pathways such as R1 and $CH_3\dot{C}HOH + O_2 = CH_3CHO + H\dot{O}_2$, respectively. Ethanol likely has a shallower blending slope than CPT due to abstraction reactions from the beta carbon forming hydroxyl-ethyl radical ($\dot{C}H_2CH_2OH$). The hydroxyl-ethyl radical can react with O_2 and form a stable peroxy adduct which proceeds through the Waddington decomposition, producing one $\dot{O}H$ radical and two formaldehyde molecules. However, as discussed in detail earlier, the $CPT\dot{O}_2J$ radical primarily produces $H\dot{O}_2$ via R1. In the case of toluene the primary fuel radical at low temperatures, benzyl ($C_6H_5\dot{C}H_2$), does not readily react with O_2 to generate $\dot{O}H$ or $H\dot{O}_2$ radicals and in the absence of abundant $H\dot{O}_2$, benzyl radicals self-recombine to form bi-benzyl, significantly inhibiting its reactivity. Therefore, toluene lacks pathways that efficiently produce $\dot{O}H$ and/or $H\dot{O}_2$ radicals in the absence of a radical generator. Hence, when blended with DME, toluene's blending slope is steeper compared to CPT and ethanol.

It is worth noting that the simulations in Figs. 6(a) and 6(b) CPT/DME blends exhibit longer ignition delay times than similar ethanol and toluene mixtures for concentrations of DME greater than 30% and 50% respectively. Based on reaction flux analysis of the models, CPT scavenges relatively more $\dot{O}H$ radicals than ethanol or toluene in their respective binary mixtures with DME at the conditions presented in Figs. 6(a) and 6(b). This potentially explains why CPT/DME mixtures are slower at higher blending concentrations of DME at these conditions. Based on the implemented H-atom abstraction rate constants by $\dot{O}H$ in each model for cyC_5H_9–H, $CH_3(CH-H)OH$, and $C_6H_5CH_2$–H sites are all within a factor of 1.4 of each other on a per H-atom basis. Additional abstractions from C–H sites in ethanol and toluene have even lower rate constants on a per H-atom basis. Therefore, we explain CPT's relatively efficient radical scavenging by noting

the number of readily abstracted hydrogen (10 secondary alkyl) compared to fewer such C–H sites for ethanol ($2 \times$ alpha, $3 \times$ beta, and $1 \times$ O–H) and toluene ($3 \times$ primary benzylic and $5 \times$ aryl).

5. Conclusions

This paper discusses the development of a reliable cyclopentane mechanism that can accurately perform in a multi-component gasoline model over a wide range of combustion relevant conditions. New IDT measurements were recorded that focused on probing the low temperature oxidation of CPT via the addition of DME. The current measurements provide valuable insights into the low temperature heat release of these binary blends. The new kinetic model developed for cyclopentane also focused on accurate kinetic description for the cyclopentene and cyclopentadiene sub-models. The model can simulate the measurements of this work well, despite the identification of reaction pathways which would benefit from future targeted experimental and theoretical studies. For instance, gaps remain in known rate constants for oxidation of cyclopentene and cyclopentadiene. Pressure dependent evaluations of published high pressure limits and new rate constants spanning engine relevant conditions ($500 \sim 2500$ K and $1 \sim 100$ bar) are also desirable for cyclopentane and its intermediates. Particularly interesting is the potential influence of the reaction of cyclopentyl-peroxy with $H\dot{O}_2$ ($CPT\dot{O}_2J + H\dot{O}_2 = CPTO_2H + O_2$) on the IDT predictions and further studies looking into this reaction are recommended. The effect on IDTs of DME addition to CPT, ethanol and toluene were compared at different temperatures. CPT was found to be relatively insensitive to DME addition up to about 60% addition compared to ethanol and toluene. The measurements and modeling presented

in this study should inform and aid in the validation of predictive models for gasoline surrogates containing cycloalkanes such as cyclopentane.

Acknowledgements

References

[1] W.J. Pitz, N.P. Cernansky, F.L. Dryer, F.N. Egolfopoulos, J.T. Farrell, D.G. Friend, H. Pitsch, Development of an Experimental Database and Chemical Kinetic Models for Surrogate Gasoline Fuels, SAE International, 2007.

[2] T.L. Alleman, R.L. McCormick, J. Yanowitz, Properties of Ethanol Fuel Blends Made with Natural Gasoline, Energ. Fuel 29 (2015) 5095-5102.

[3] S.J. Eaton, S.H. Beis, S.A. Karunarathne, H.P. Pendse, M.C. Wheeler, Hydroprocessing of Biorenewable Thermal Deoxygenation Oils, Energ. Fuel 29 (2015) 3224-3232.

[4] C.S. McEnally, L.D. Pfefferle, Experimental study of fuel decomposition and hydrocarbon growth processes for cyclohexane and related compounds in nonpremixed flames, Combustion and Flame 136 (2004) 155-167.

[5] C.S. McEnally, D.D. Das, L.D. Pfefferle, Yield Sooting Index Database Volume 2: Sooting Tendencies of a Wide Range of Fuel Compounds on a Unified Scale, Harvard Dataverse, 2017.

[6] M.J. Al Rashidi, S. Thion, C. Togbé, G. Dayma, M. Mehl, P. Dagaut, W.J. Pitz, J. Zádor, S.M. Sarathy, Elucidating reactivity regimes in cyclopentane oxidation: Jet stirred reactor experiments, computational chemistry, and kinetic modeling, Proc. Combust. Inst 36 (2017) 469-477.

[7] M.J. Al Rashidi, J.C. Mármol, C. Banyon, M.B. Sajid, M. Mehl, W.J. Pitz, S. Mohamed, A. Alfazazi, T. Lu, H.J. Curran, A. Farooq, S.M. Sarathy, Cyclopentane combustion. Part II. Ignition delay measurements and mechanism validation, Combust. Flame 183 (2017) 372-385.

[8] J.B. Randazzo, C.J. Annesley, K. Bell, R.S. Tranter, A shock tube laser schlieren study of cyclopentane pyrolysis, Proc. Combust. Inst 36 (2017) 273-280.

[9] M.V. Khandavilli, F.H. Vermeire, R. Van de Vijver, M. Djokic, H.-H. Carstensen, K.M. Van Geem, G.B. Marin, Group additive modeling of cyclopentane pyrolysis, J. Anal. Appl. Pyrol 128 (2017) 437-450.

[10] S.G. Davis, C.K. Law, Determination of and Fuel Structure Effects on Laminar Flame Speeds of C1 to C8 Hydrocarbons, Combust. Sci. Technol. 140 (1998) 427-449.

[11] H. Zhao, J. Wang, X. Cai, Z. Tian, Q. Li, Z. Huang, A comparison study of cyclopentane and cyclohexane laminar flame speeds at elevated pressures and temperatures, Fuel 234 (2018) 238-246.

[12] Z. Tian, C. Tang, Y. Zhang, J. Zhang, Z. Huang, Shock Tube and Kinetic Modeling Study of Cyclopentane and Methylcyclopentane, Energ. Fuel 29 (2015) 428-441.

[13] B. Sirjean, F. Buda, H. Hakka, P.A. Glaude, R. Fournet, V. Warth, F. Battin-Leclerc, M. Ruiz-Lopez, The autoignition of cyclopentane and cyclohexane in a shock tube, Proc. Combust. Inst 31 (2007) 277-284.

[14] S.M. Daley, A.M. Berkowitz, M.A. Oehlschlaeger, A shock tube study of cyclopentane and cyclohexane ignition at elevated pressures, Int. J. Chem. Kinet. 40 (2008) 624-634.

[15] A. Fridlyand, S.S. Goldsborough, M. Al Rashidi, S.M. Sarathy, M. Mehl, W.J. Pitz, Low temperature autoignition of 5-membered ring naphthenes: Effects of substitution, Combust. Flame 200 (2019) 387-404.

[16] G. Dayma, S. Thion, Z. Serinyel, P. Dagaut, EXPERIMENTAL AND KINETIC MODELLING STUDY OF THE OXIDATION OF CYCLOPENTANE AND METHYLCYCLOPENTANE AT ATMOSPHERIC PRESSURE, 11th Mediterranean Combustion Symposium, Tenerife, Spain, 2019.

[17] D. Kang, A. Fridlyand, S.S. Goldsborough, S.W. Wagnon, M. Mehl, W.J. Pitz, M.J. McNenly, Auto-ignition study of FACE gasoline and its surrogates at advanced IC engine conditions, Proc. Combust. Inst 37 (2019) 4699-4707.

[18] S.M. Sarathy, G. Kukkadapu, M. Mehl, T. Javed, A. Ahmed, N. Naser, A. Tekawade, G. Kosiba, M. AlAbbad, E. Singh, S. Park, M.A. Rashidi, S.H. Chung, W.L. Roberts, M.A. Oehlschlaeger, C.-J. Sung, A. Farooq, Compositional effects on the ignition of FACE gasolines, Combust. Flame 169 (2016) 171-193.

[19] Y. Zhang, H. El-Merhubi, B. Lefort, L. Le Moyne, H.J. Curran, A. Kéromnès, Probing the low-temperature chemistry of ethanol via the addition of dimethyl ether, Combust. Flame 190 (2018) 74-86.

[20] Y. Zhang, K.P. Somers, M. Mehl, W.J. Pitz, R.F. Cracknell, H.J. Curran, Probing the antagonistic effect of toluene as a component in surrogate fuel models at low temperatures and high pressures. A case study of toluene/dimethyl ether mixtures, Proc. Combust. Inst 36 (2017) 413-421.

[21] E.L. Petersen, M.J.A. Rickard, M.W. Crofton, E.D. Abbey, M.J. Traum, D.M. Kalitan, A facility for gas- and condensed-phase measurements behind shock waves, Measurement Science and Technology 16 (2005) 1716-1729.

[22] M. Baigmohammadi, V. Patel, S. Martinez, S. Panigrahy, A. Ramalingam, U. Burke, K.P. Somers, K.A. Heufer, A. Pekalski, H.J. Curran, Comprehensive Experimental and Simulation Study of Ignition Delay Time Characteristics of Single Fuel C1–C2 Hydrocarbons over a Wide Range of Temperatures, Pressures, Equivalence Ratios, and Dilutions, Energy & Fuels 34 (2020) 3755-3771.

[23] B.W. Weber, C.-J. Sung, M.W. Renfro, On the uncertainty of temperature estimation in a rapid compression machine, Combust. Flame 162 (2015) 2518-2528.

[24] C. Morley, Gaseq, http://www.gaseq.co.uk/ (2004).

[25] S. Yousefian, N.J. Quinlan, R.F.D. Monaghan, Simulation of turbulent flow in a rapid compression machine: Large Eddy Simulation and computationally efficient alternatives for the design of ignition delay time experiments, Fuel 234 (2018) 30-47.

[26] Y. Li, C.-W. Zhou, K.P. Somers, K. Zhang, H.J. Curran, The oxidation of 2-butene: A high pressure ignition delay, kinetic modeling study and reactivity comparison with isobutene and 1-butene, Proc. Combust. Inst 36 (2017) 403-411.

[27] M.J. Al Rashidi, M. Mehl, W.J. Pitz, S. Mohamed, S.M. Sarathy, Cyclopentane combustion chemistry. Part I: Mechanism development and computational kinetics, Combust. Flame 183 (2017) 358-371.

[28] G. Kukkadapu, D. Kang, S.W. Wagnon, K. Zhang, M. Mehl, M. Monge-Palacios, H. Wang, S.S. Goldsborough, C.K. Westbrook, W.J. Pitz, Kinetic modeling study of surrogate components for gasoline, jet and diesel fuels: C7-C11 methylated aromatics, Proc. Combust. Inst 37 (2019) 521-529.

[29] E.R. Ritter, J.W. Bozzelli, THERM: Thermodynamic property estimation for gas phase radicals and molecules, Int. J. Chem. Kinet. 23 (1991) 767-778.

[30] S.M. Burke, J.M. Simmie, H.J. Curran, Critical Evaluation of Thermochemical Properties of C1–C4 Species: Updated Group-Contributions to Estimate Thermochemical Properties, J. Phys. Chem. Ref. Data 44 (2015) 013101.

[31] Y. Li, H.J. Curran, Extensive Theoretical Study of the Thermochemical Properties of Unsaturated Hydrocarbons and Allylic and Super-Allylic Radicals: The Development and Optimization of Group Additivity Values, J. Phys. Chem. A 122 (2018) 4736-4749.

[32] S.W. Wagnon, S. Thion, E.J.K. Nilsson, M. Mehl, Z. Serinyel, K. Zhang, P. Dagaut, A.A. Konnov, G. Dayma, W.J. Pitz, Experimental and modeling studies of a biofuel surrogate compound: laminar burning velocities and jet-stirred reactor measurements of anisole, Combust. Flame 189 (2018) 325-336.

[33] S. Dooley, M. Uddi, S.H. Won, F.L. Dryer, Y. Ju, Methyl butanoate inhibition of n-heptane diffusion flames through an evaluation of transport and chemical kinetics, Combust. Flame 159 (2012) 1371-1384.

[34] R. Bosque, J. Sales, Polarizabilities of Solvents from the Chemical Composition, J. Chem. Inform. Comput. Sci. 42 (2002) 1154-1163.

[35] M.J. McNenly, R.A. Whitesides, D.L. Flowers, Faster solvers for large kinetic mechanisms using adaptive preconditioners, Proc. Combust. Inst 35 (2015) 581-587.

[36] B. Sirjean, P.A. Glaude, M.F. Ruiz-Lopez, R. Fournet, Detailed Kinetic Study of the Ring Opening of Cycloalkanes by CBS-QB3 Calculations, J. Phys. Chem. A 110 (2006) 12693-12704.

[37] W. Tsang, Thermal decomposition of cyclopentane and related compounds, Int. J. Chem. Kinet. 10 (1978) 599-617.

[38] J.H. Kiefer, K.S. Gupte, L.B. Harding, S.J. Klippenstein, Shock Tube and Theory Investigation of Cyclohexane and 1-Hexene Decomposition, J. Phys. Chem. A 113 (2009) 13570-13583.

[39] H.-H. Carstensen, A.M. Dean, Rate Constant Rules for the Automated Generation of Gas-Phase Reaction Mechanisms, J. Phys. Chem. A 113 (2009) 367-380.

[40] N. Cohen, K.R. Westberg, Chemical Kinetic Data Sheets for High-Temperature Reactions. Part II, J. Phys. Chem. Ref. Data 20 (1991) 1211-1311.

[41] R. Sivaramakrishnan, J.V. Michael, Shock tube measurements of high temperature rate constants for OH with cycloalkanes and methylcycloalkanes, Combust. Flame 156 (2009) 1126-1134.

[42] D.L. Baulch, C.J. Cobos, R.A. Cox, C. Esser, P. Frank, T. Just, J.A. Kerr, M.J. Pilling, J. Troe, R.W. Walker, J. Warnatz, Evaluated kinetic data for combustion modelling, Journal of Physical Chemical Reference Data 21 (1992) 411.

[43] N.K. Srinivasan, M.-C. Su, J.W. Sutherland, J.V. Michael, Reflected shock tube studies of high-temperature rate constants for $CH_3 + O_2$, $H_2CO + O_2$, and $OH + O_2$, Journal of Physical Chemistry A 109 (2005) 7902-7914.

[44] J. Aguilera-Iparraguirre, H.J. Curran, W. Klopper, J.M. Simmie, Accurate Benchmark Calculation of the Reaction Barrier Height for Hydrogen Abstraction by the Hydroperoxyl Radical from Methane. Implications for CnH2n+2 where n = 2 → 4, J. Phys. Chem. A 112 (2008) 7047-7054.

[45] J.A. Manion, I.A. Awan, A Shock Tube Study of H Atom Addition to Cyclopentene, Int. J. Chem. Kinet. 50 (2018) 225-242.

[46] K. Zhang, C. Banyon, H.J. Curran, A. Rodriguez, O. Herbinet, F. Battin-Leclerc, C. B'Chir, K.A. Heufer, An updated experimental and kinetic modeling study of n-heptane oxidation, Combustion and Flame 172 (2016) 116-135.

[47] C.F. Goldsmith, M.P. Burke, Y. Georgievskii, S.J. Klippenstein, Effect of non-thermal product energy distributions on ketohydroperoxide decomposition kinetics, Proceedings of the Combustion Institute 35 (2015) 283-290.

[48] A.W. Jasper, S.J. Klippenstein, L.B. Harding, Theoretical rate coefficients for the reaction of methyl radical with hydroperoxyl radical and for methylhydroperoxide decomposition, Proceedings of the Combustion Institute 32 (2009) 279-286.

[49] K. Wang, S.M. Villano, A.M. Dean, Fundamentally-based kinetic model for propene pyrolysis, Combust. Flame 162 (2015) 4456-4470.

[50] D.K. Lewis, J. Bergmann, R. Manjoney, R. Paddock, B.L. Kalra, Rates of reactions of cyclopropane, cyclobutane, cyclopentene,and cyclohexene in the presence of boron trichloride, J. Phys. Chem. 88 (1984) 4112-4116.

[51] J.E. Baldwin, Thermal Rearrangements of Vinylcyclopropanes to Cyclopentenes, Chem. Rev. 103 (2003) 1197-1212.

[52] D.K. Lewis, D.J. Charney, B.L. Kalra, A.-M. Plate, M.H. Woodard, S.J. Cianciosi, J.E. Baldwin, Kinetics of the Thermal Isomerizations of Gaseous Vinylcyclopropane and Vinylcyclobutane, J. Phys. Chem. A 101 (1997) 4097-4102.

[53] C.A. Wellington, THE THERMAL ISOMERIZATION OF VINYLCYCLOPROPANE, J. Phys. Chem. 66 (1962) 1671-1674.

[54] L.B. Harding, S.J. Klippenstein, Y. Georgievskii, On the Combination Reactions of Hydrogen Atoms with Resonance-Stabilized Hydrocarbon Radicals, J. Phys. Chem. A 111 (2007) 3789-3801.

[55] F. Leonori, N. Balucani, V. Nevrly, A. Bergeat, S. Falcinelli, G. Vanuzzo, P. Casavecchia, C. Cavallotti, Experimental and Theoretical Studies on the Dynamics of the O(3P) + Propene Reaction: Primary Products, Branching Ratios, and Role of Intersystem Crossing, J. Phys. Chem. C 119 (2015) 14632-14652.

[56] R.K. Robinson, R.P. Lindstedt, On the chemical kinetics of cyclopentadiene oxidation, Combust. Flame 158 (2011) 666-686.

[57] S.S. Vasu, L.K. Huynh, D.F. Davidson, R.K. Hanson, D.M. Golden, Reactions of OH with Butene Isomers: Measurements of the Overall Rates and a Theoretical Study, J. Phys. Chem. A 115 (2011) 2549-2556.

[58] J. Zádor, S.J. Klippenstein, J.A. Miller, Pressure-Dependent OH Yields in Alkene + HO2 Reactions: A Theoretical Study, J. Phys. Chem. A 115 (2011) 10218-10225.

[59] D.L. Baulch, C.J. Cobos, R.A. Cox, P. Frank, G. Hayman, T. Just, J.A. Kerr, T. Murrells, M.J. Pilling, J. Troe, R.W. Walker, J. Warnatz, Evaluated Kinetic Data for Combustion Modeling. Supplement I, Journal of Physical and Chemical Reference Data 23 (1994) 847.

[60] K. Wang, S.M. Villano, A.M. Dean, Reactivity-structure-based rate estimation rules for alkyl radical H atom shift and alkenyl radical cycloaddition reactions, Journal of Physical Chemistry A 119 (2015) 7205-7221.

[61] K. Wang, S.M. Villano, A.M. Dean, The impact of resonance stabilization on the intramolecular hydrogen-atom shift reactions of hydrocarbon radicals, ChemPhysChem 16 (2015) 2635-2645.

[62] C.-W. Zhou, J.M. Simmie, K.P. Somers, C.F. Goldsmith, H.J. Curran, Chemical kinetics of hydrogen atom abstraction from allylic sites by $^3O_2$; Implications for combustion modeling and simulation, Journal of Physical Chemistry A 121 (2017) 1890-1899.

[63] K. Wang, S.M. Villano, A.M. Dean, Reactions of allylic radicals that impact molecular weight growth kinetics, Phys. Chem. Chem. Phys 17 (2015) 6255-6273.

[64] J. Zádor, A.W. Jasper, J.A. Miller, The reaction between propene and hydroxyl, Phys. Chem. Chem. Phys 11 (2009) 11040-11053.

[65] C. Cavallotti, D. Polino, On the kinetics of the $C_5H_5+C_5H_5$ reaction, Proc. Combust. Inst 34 (2013) 557-564.

[66] P.T. Lynch, C.J. Annesley, C.J. Aul, X. Yang, R.S. Tranter, Recombination of Allyl Radicals in the High Temperature Fall-Off Regime, J. Phys. Chem. A 117 (2013) 4750-4761.

[67] A.R. Ghildina, A.D. Oleinikov, V.N. Azyazov, A.M. Mebel, Reaction mechanism, rate constants, and product yields for unimolecular and H-assisted decomposition of 2,4-cyclopentadienone and oxidation of cyclopentadienyl with atomic oxygen, Combust. Flame 183 (2017) 181-193.

[68] C.F. Goldsmith, S.J. Klippenstein, W.H. Green, Theoretical rate coefficients for allyl+HO2 and allyloxy decomposition, Proc. Combust. Inst 33 (2011) 273-282.

[69] K. Wang, S.M. Villano, A.M. Dean, Ab initio study of the influence of resonance stabilization on intramolecular ring closure reactions of hydrocarbon radicals, Phys. Chem. Chem. Phys 18 (2016) 8437-8452.

[70] H. Sun, J.W. Bozzelli, C.K. Law, Thermochemical and Kinetic Analysis on the Reactions of O2 with Products from OH Addition to Isobutene, 2-Hydroxy-1,1-dimethylethyl, and 2-Hydroxy-2-methylpropyl Radicals: HO2 Formation from Oxidation of Neopentane, Part II, J. Phys. Chem. A 111 (2007) 4974-4986.

[71] K. Mahmud, P. Marshall, A. Fontijn, A high-temperature photochemistry kinetics study of the reaction of oxygen(3P) atoms with ethylene from 290 to 1510 K, J. Phys. Chem. 91 (1987) 1568-1573.

[72] J.A. Miller, S.J. Klippenstein, Dissociation of Propyl Radicals and Other Reactions on a C3H7 Potential, J. Phys. Chem. A 117 (2013) 2718-2727.

[73] J.P. Senosiain, S.J. Klippenstein, J.A. Miller, Reaction of Ethylene with Hydroxyl Radicals: A Theoretical Study, J. Phys. Chem. A 110 (2006) 6960-6970.

[74] K. Nakamura, S. Koda, Reaction of atomic oxygen with cyclopentadiene, Int. J. Chem. Kinet. 9 (1977) 67-81.

[75] C. Cavallotti, F. Leonori, N. Balucani, V. Nevrly, A. Bergeat, S. Falcinelli, G. Vanuzzo, P. Casavecchia, Relevance of the Channel Leading to Formaldehyde + Triplet Ethylidene in the O(3P) + Propene Reaction under Combustion Conditions, J. Phys. Chem. Lett. 5 (2014) 4213-4218.

[76] X. Zhong, J.W. Bozzelli, Thermochemical and kinetic analysis on the addition reactions of H, O, OH, and HO2 with 1,3-cyclopentadiene, International Journal of Chemical Kinetics 29 (1997) 893-913.

[77] G.R. Galimova, V.N. Azyazov, A.M. Mebel, Reaction mechanism, rate constants, and product yields for the oxidation of Cyclopentadienyl and embedded five-member ring radicals with hydroxyl, Combust. Flame 187 (2018) 147-164.

[78] A.D. Oleinikov, V.N. Azyazov, A.M. Mebel, Oxidation of cyclopentadienyl radical with molecular oxygen: A theoretical study, Combust. Flame 191 (2018) 309-319.

[79] S. Sharma, W.H. Green, Computed Rate Coefficients and Product Yields for c-C5H5 + CH3 → Products, J. Phys. Chem. A 113 (2009) 8871-8882.

[80] F. Dubnikova, A. Lifshitz, Ring Expansion in Methylcyclopentadiene Radicals. Quantum Chemical and Kinetics Calculations, J. Phys. Chem. A 106 (2002) 8173-8183.

[81] G. da Silva, Mystery of 1-Vinylpropargyl Formation from Acetylene Addition to the Propargyl Radical: An Open-and-Shut Case, J. Phys. Chem. A 121 (2017) 2086-2095.

[82] D.K. Hahn, S.J. Klippenstein, J.A. Miller, A theoretical analysis of the reaction between propargyl and molecular oxygen, Faraday Discussions 119 (2002) 79-100.

[83] S. Yommee, J.W. Bozzelli, Cyclopentadienone Oxidation Reaction Kinetics and Thermochemistry for the Alcohols, Hydroperoxides, and Vinylic, Alkoxy, and Alkylperoxy Radicals, J. Phys. Chem. A 120 (2016) 433-451.

[84] O. Herbinet, A. Rodriguez, B. Husson, F. Battin-Leclerc, Z. Wang, Z. Cheng, F. Qi, Study of the Formation of the First Aromatic Rings in the Pyrolysis of Cyclopentene, J. Phys. Chem. A 120 (2016) 668-682.

[85] U. Burke, K.P. Somers, P. O'Toole, C.M. Zinner, N. Marquet, G. Bourque, E.L. Petersen, W.K. Metcalfe, Z. Serinyel, H.J. Curran, An ignition delay and kinetic modeling study of methane, dimethyl ether, and their mixtures at high pressures, Combust. Flame 162 (2015) 315-330.

[86] M. Yahyaoui, M.H. Hakka, P.A. Glaude, F. Battin-Leclerc, Experimental and modeling study of the autoignition of cyclopentene, Int. J. Chem. Kinet. 40 (2008) 25-33.

[87] Z. Li, W. Wang, Z. Huang, M.A. Oehlschlaeger, Dimethyl Ether Autoignition at Engine-Relevant Conditions, Energ. Fuel 27 (2013) 2811-2817.

[88] U. Pfahl, K. Fieweger, G. Adomeit, Self-ignition of diesel-relevant hydrocarbon-air mixtures under engine conditions, Symp. Combust. 26 (1996) 781-789.

[89] A. Miyoshi, SI Combustion Characteristics of Cyclopentane - Detailed Kinetic Mechanism, SAE International, 2019.